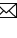


# Supplementary Information

## A Blockchain Consensus Mechanism for Real-Time Regulation of Renewable Energy Power Systems

Yi Yu<sup>1,2,3</sup>, Guo-Ping Liu<sup>1,2</sup>, Yi Huang<sup>4</sup>, Chi Yung Chung<sup>3</sup>, Yu-Zhong Li<sup>5</sup>

This file is a supplement to the original paper, which includes supplementary figures, supplementary algorithms, supplementary tables, and supplementary notes. In particular, the mechanisms for searching and verifying candidate solutions in PoT are elaborated in the supplementary notes. Furthermore, the specific implementations of three applications are detailed in these supplementary notes, including two PoT-based applications and one DPoT-based application.


<sup>1</sup>Shenzhen Key Laboratory of Control Theory and Intelligent Systems, Southern University of Science and Technology, Shenzhen 518055, China.

<sup>2</sup>Center for Control Science and Technology, Southern University of Science and Technology, Shenzhen 518055, China.

<sup>3</sup>Department of Electrical and Electronic Engineering and Research Centre for Grid Modernisation, The Hong Kong Polytechnic University, Hong Kong SAR, China.

<sup>4</sup>School of Electrical Engineering and Automation, Wuhan University, Wuhan 430072, China.

<sup>5</sup>School of Computer Science and Engineering, Huizhou University, Huizhou 516007, China.

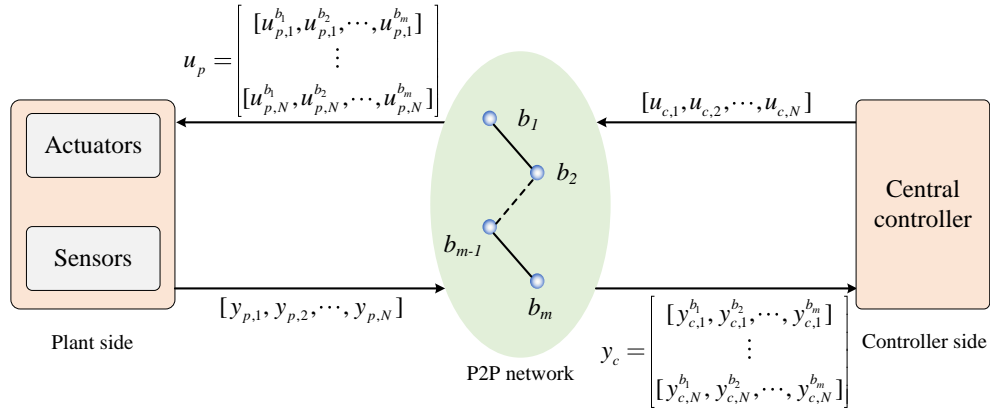
Correspondence: liugp@sustech.edu.cn.

## CONTENTS

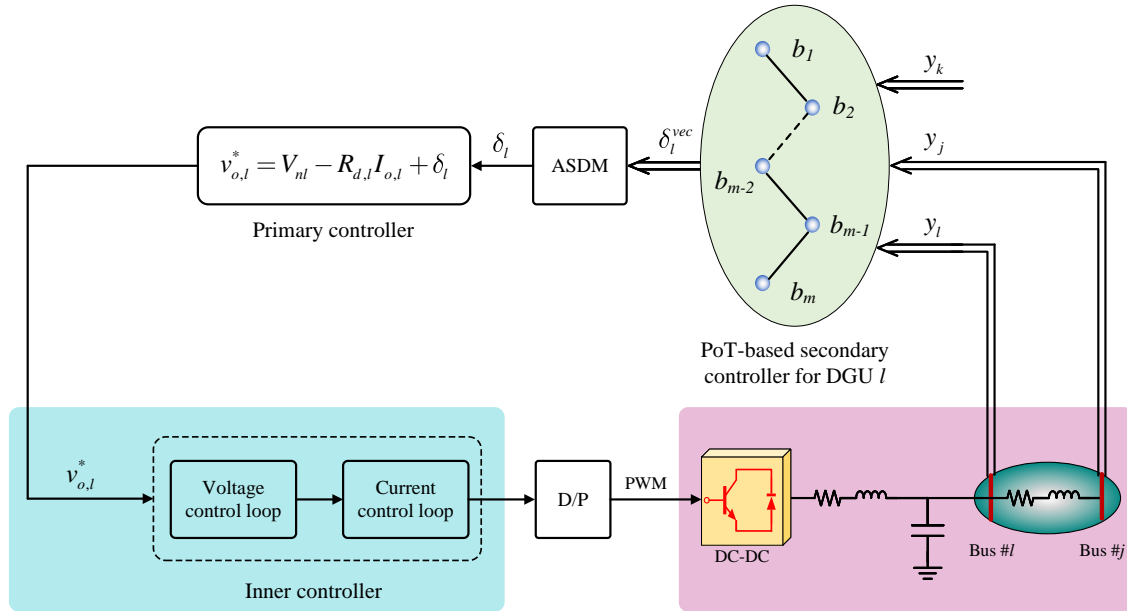
<b>I</b>	<b>Supplementary Figures</b>	3
<b>II</b>	<b>Supplementary Algorithms</b>	16
<b>III</b>	<b>Supplementary Tables</b>	17
<b>IV</b>	<b>Supplementary Note 1: Preliminaries for Blockchain</b>	20
<b>V</b>	<b>Supplementary Note 2: Searching and Verifying Solutions to a Regulation Problem</b>	21
<b>VI</b>	<b>Supplementary Note 3: PoT-Based Distributed Secondary Regulation Strategy</b>	23
	VI-A Abbreviation . . . . .	23
	VI-B Variable and Parameter . . . . .	23
	VI-C System Model of DC Microgrids . . . . .	23
	VI-D Regulation Objectives of DC microgrids . . . . .	24
	VI-E Dynamics of Multi-Bus DC Microgrids . . . . .	24
	VI-F PoT-Based Secondary Regulation Strategy . . . . .	26
<b>VII</b>	<b>Supplementary Note 4: PoT-Based Distributed Load Frequency Control Strategy</b>	29
	VII-A Abbreviation . . . . .	29
	VII-B Variable and Parameter . . . . .	29
	VII-C System Model of Multi-Area Interconnected Power System . . . . .	29
	VII-D PoT-Based Distributed Load Frequency Control Strategy . . . . .	30
<b>VIII</b>	<b>Supplementary Note 5: DPoT-Based Centralized Secondary Regulation Strategy</b>	33
	<b>Supplementary References</b>	34

## I. SUPPLEMENTARY FIGURES

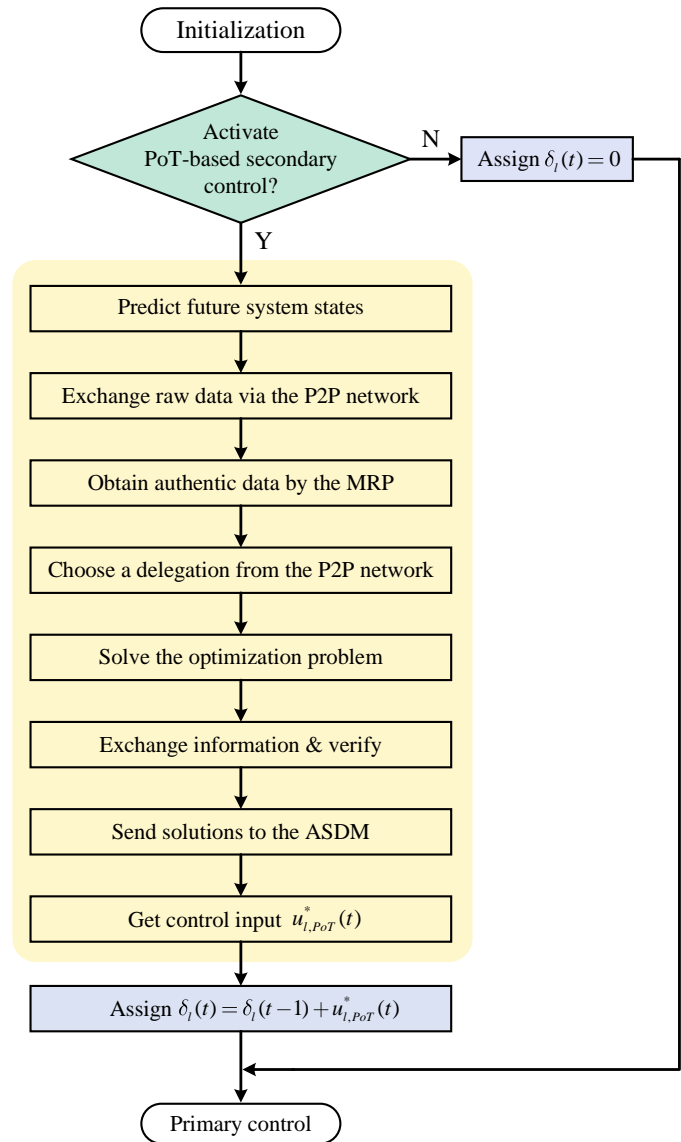
Here are the supplementary figures used in the main text.



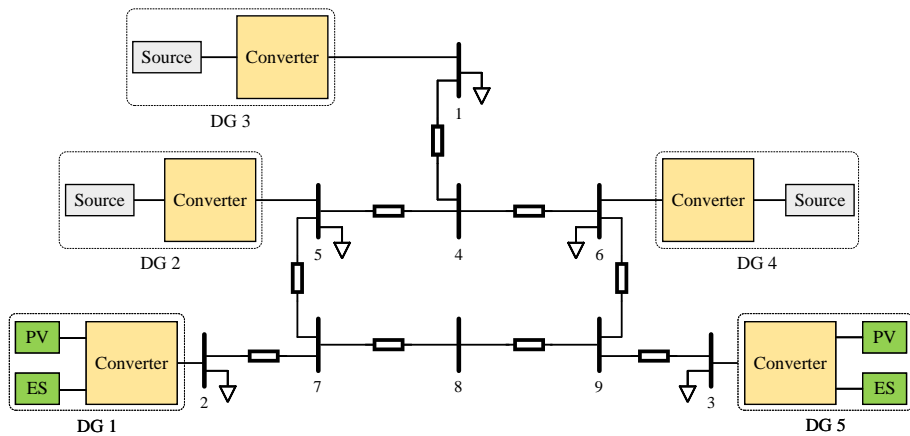
Supplementary Figure 1: Architecture of a renewable energy power system with the PFC-based regulation strategy.



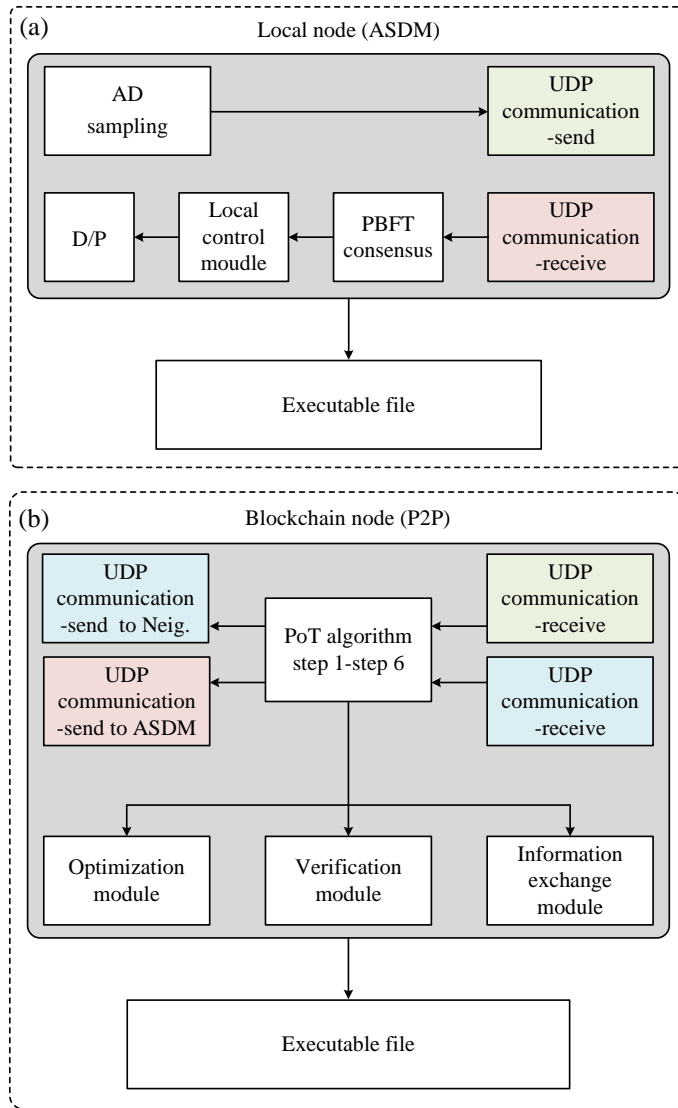
Supplementary Figure 2: Architecture of the multi-bus DC microgrid system with the PoT-based secondary regulation strategy. D/P stands for PWM generator.



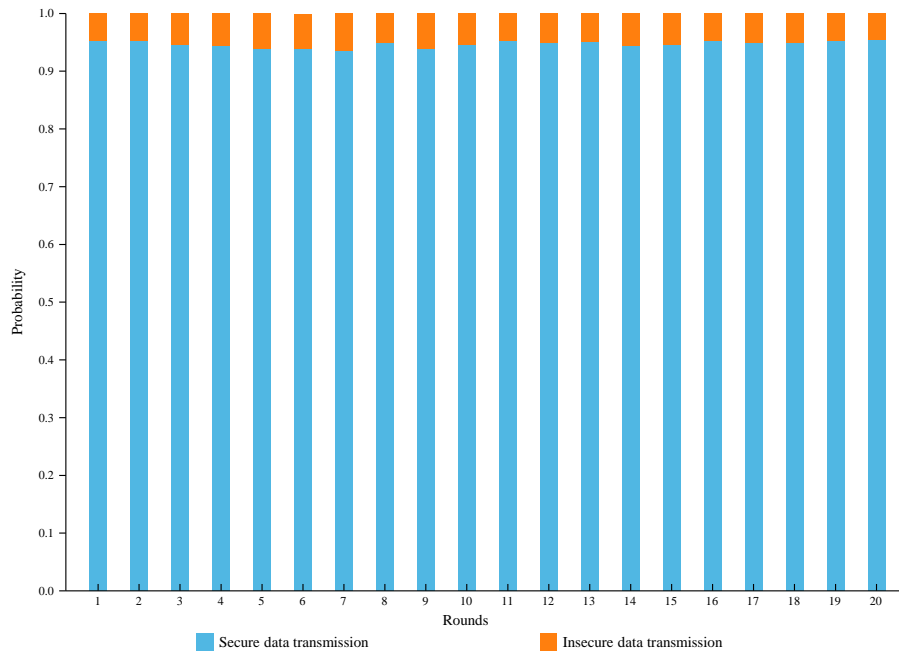
Supplementary Figure 3: The flowchart of the PoT-based secondary regulation strategy for DC microgrids.



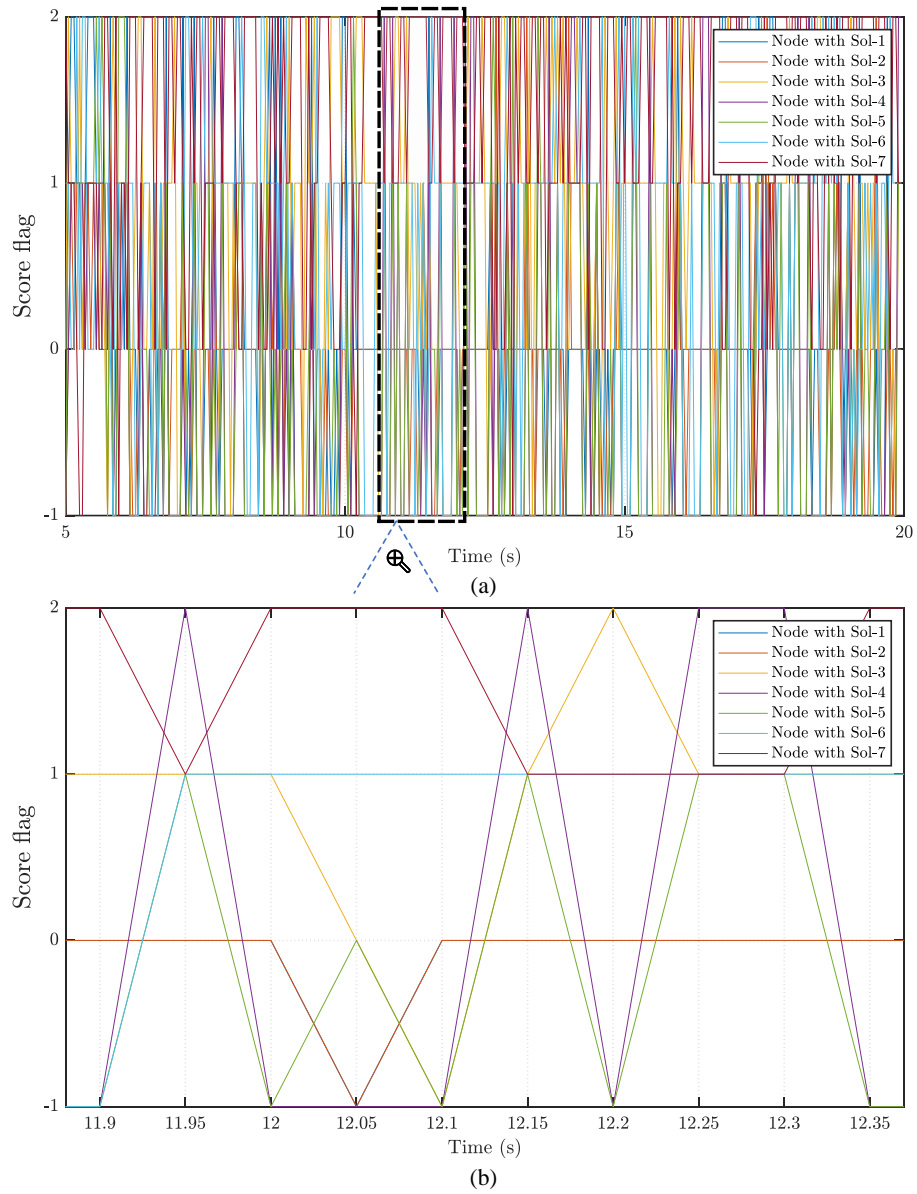
Supplementary Figure 4: Block diagram of the electrical part of the IEEE 9-bus system with five power generation units.



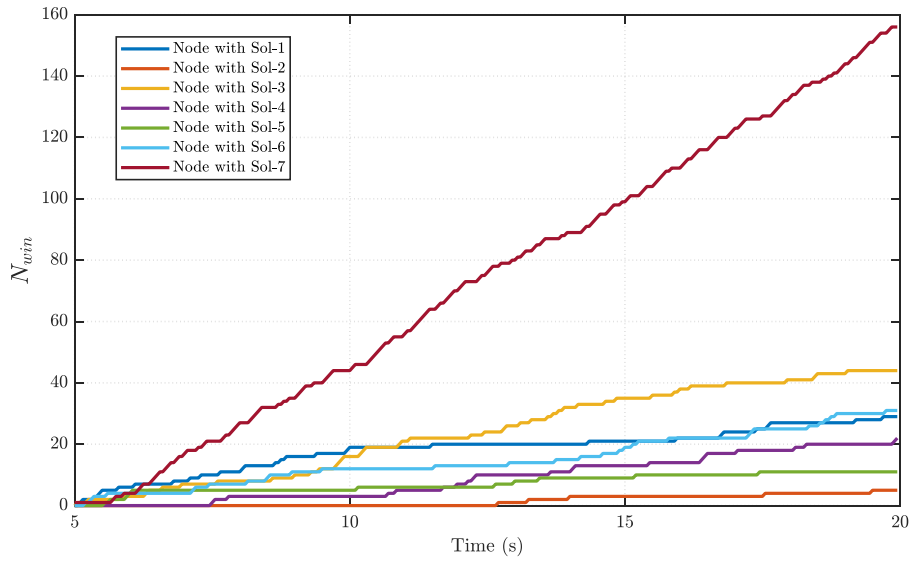
Supplementary Figure 5: PoT code structure for Application 1. PBFT stands for Practical Byzantine Fault Tolerance.



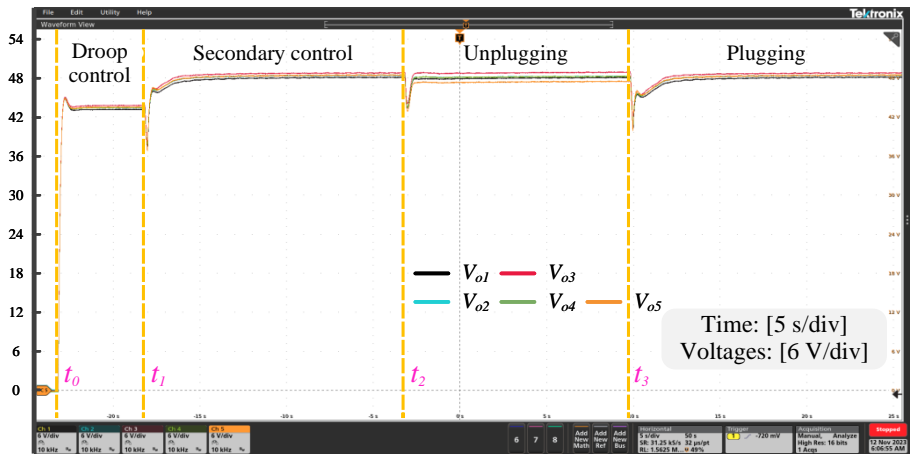
Supplementary Figure 6: Ratio of probability of successful defense w.r.t. probability of unsuccessful defense for DC microgrids under PoT-based secondary control over 20 independent repeated trials (Application 1).



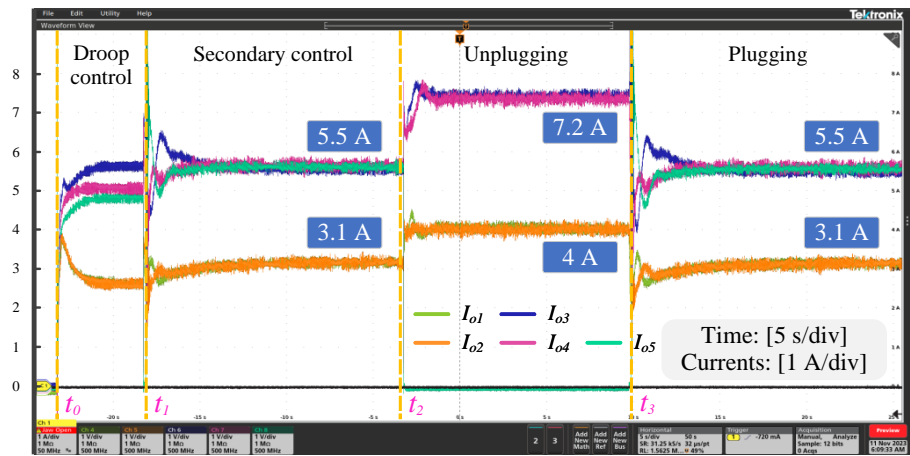
Supplementary Figure 7: The performance of the solver at each node throughout the PoT-based secondary control process. The meanings of 'Sol-1~Sol-7' in the legends are given in the Supplementary Table 7. The values of 'Score flag' are  $-1$ ,  $0$ ,  $1$  and  $2$ . The meanings of these four values are shown in the Supplementary Table 8.



Supplementary Figure 8: The cumulative number  $N_{win}$  of times each node wins PoT consensus throughout the control process, i.e., the number of times ‘Score flag’ takes the value of 2.



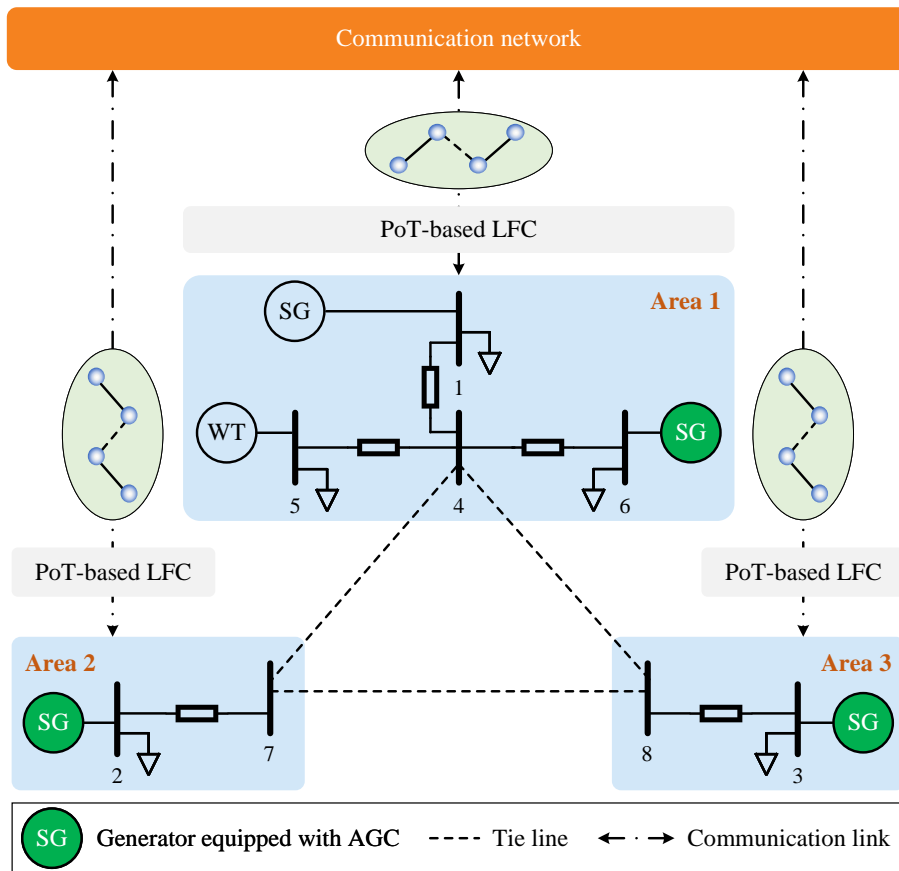
(a)



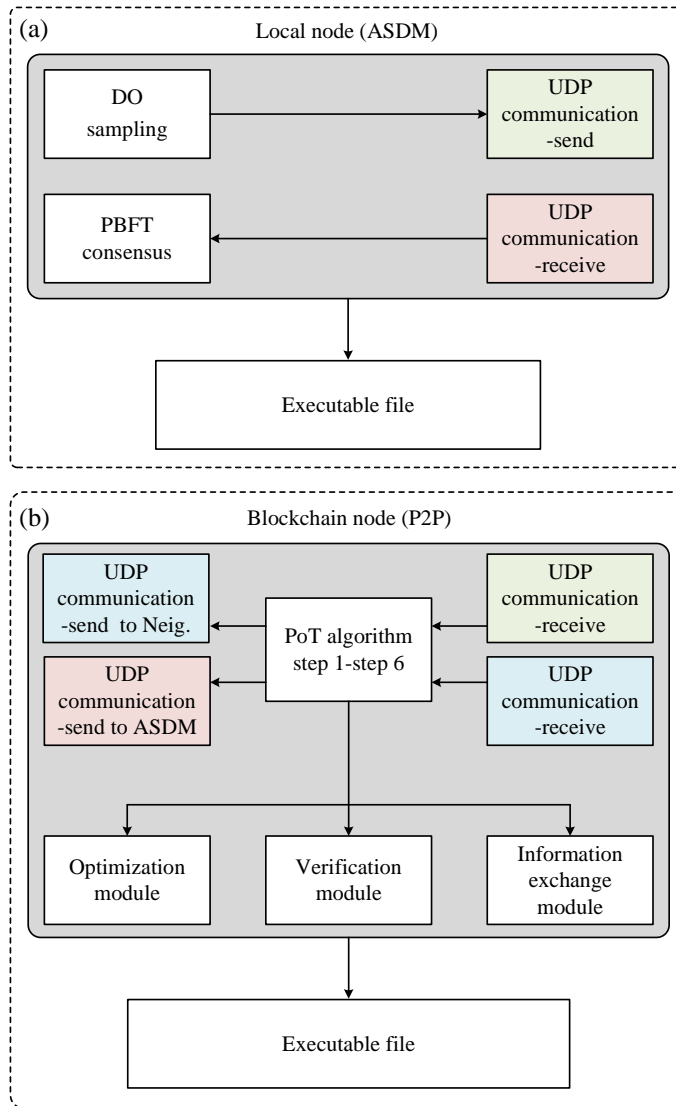
(b)

Supplementary Figure 9: Microgrid responses under the PoT-based approach for the plug-and-play scenario. (a) Measured voltages at the Point of Common Coupling (PCC). (b) Output currents of DGUs (Application 1).

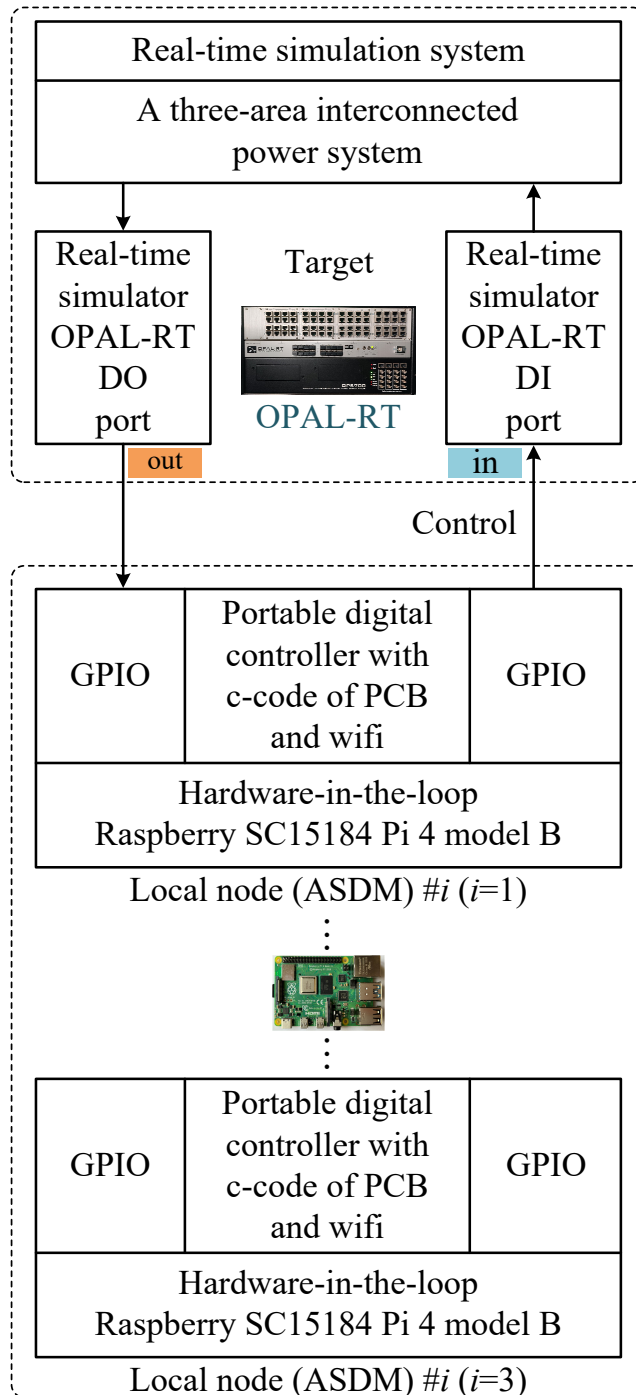




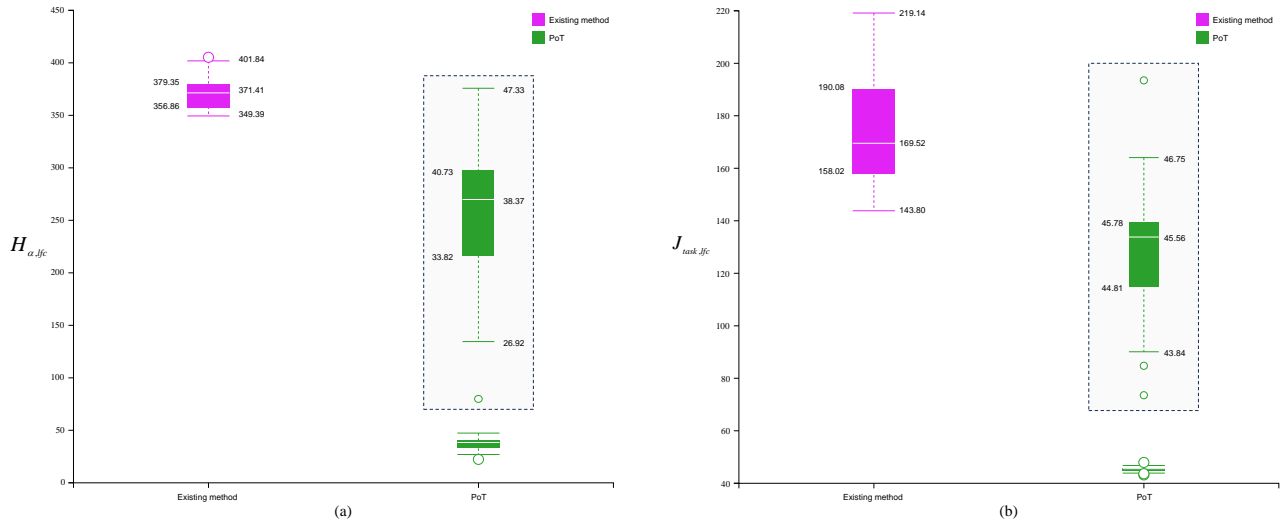
Supplementary Figure 10: Block diagram of a three-area interconnected power system with the PoT-based LFC strategy, where SG, WT, and AGC represents synchronous generators, wind turbines, and automatic generation control, respectively.



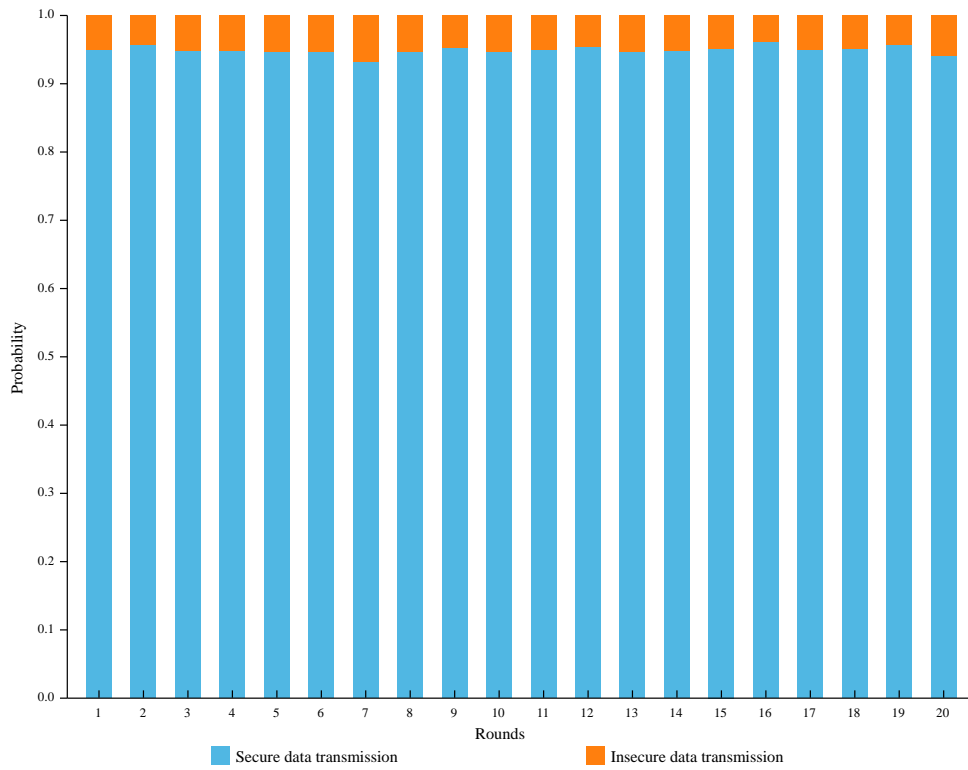
Supplementary Figure 11: PoT code structure for Application 2. DO refers to the digital output.



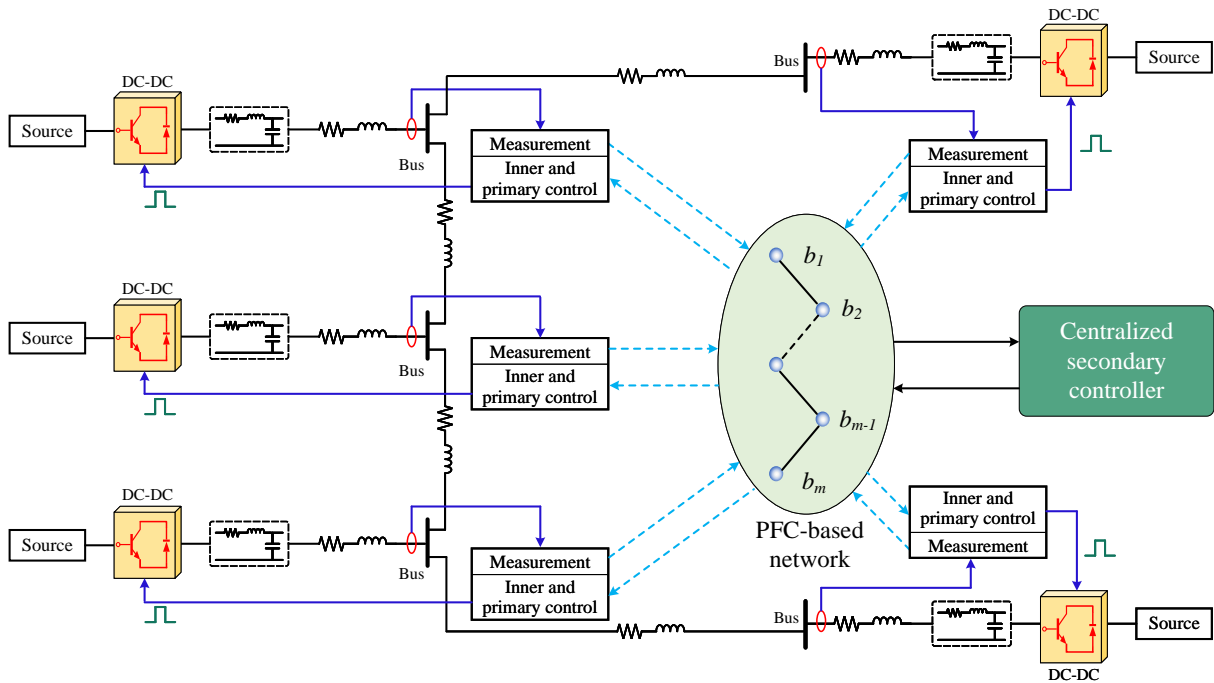
Supplementary Figure 12: Architecture of the HIL test system in Application 2. DO and DI respectively refer to the digital output and digital input.



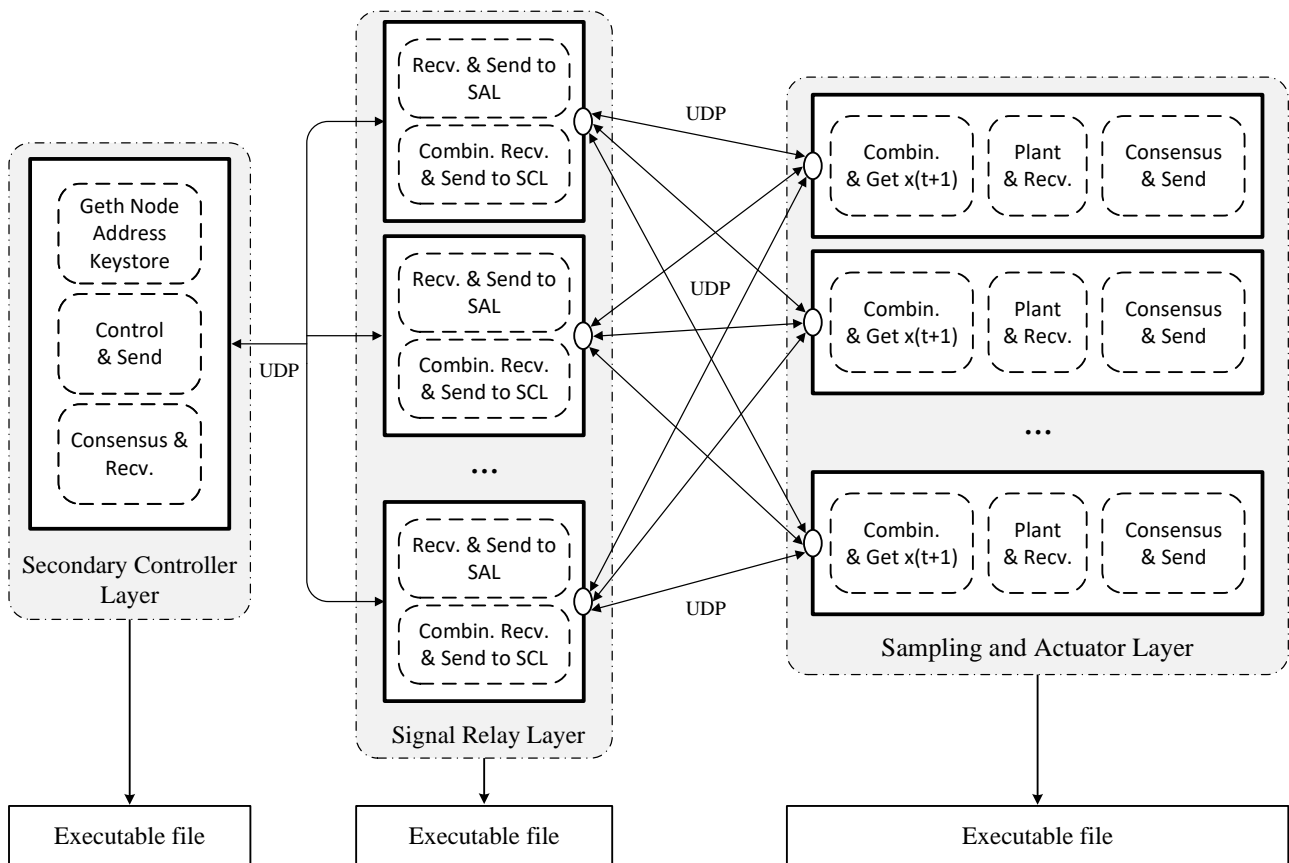
Supplementary Figure 13: Comparison of the performance metrics of the tested three-area power system under different approaches: (a) the security performance index  $H_{\alpha, lfc}$ , (b) the control performance index  $J_{task, lfc}$ . The middle part of the figure shows two enlarged subplots. The method labeled as ‘Existing method’ corresponds to the approach in [57] of the paper (Application 2).



Supplementary Figure 14: Ratio of probability of successful defense w.r.t. probability of unsuccessful defense for the tested three-area power system under PoT-based LFC over 20 independent repeated trials (Application 2).

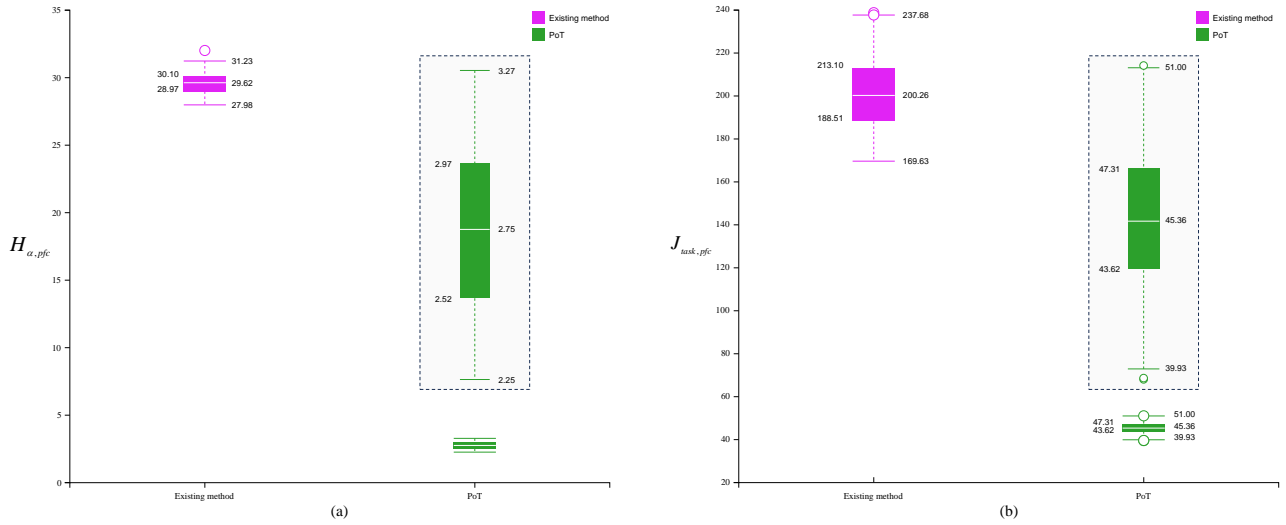


Supplementary Figure 15: The architecture of the DC microgrid with PFC-based secondary control (Application 3).

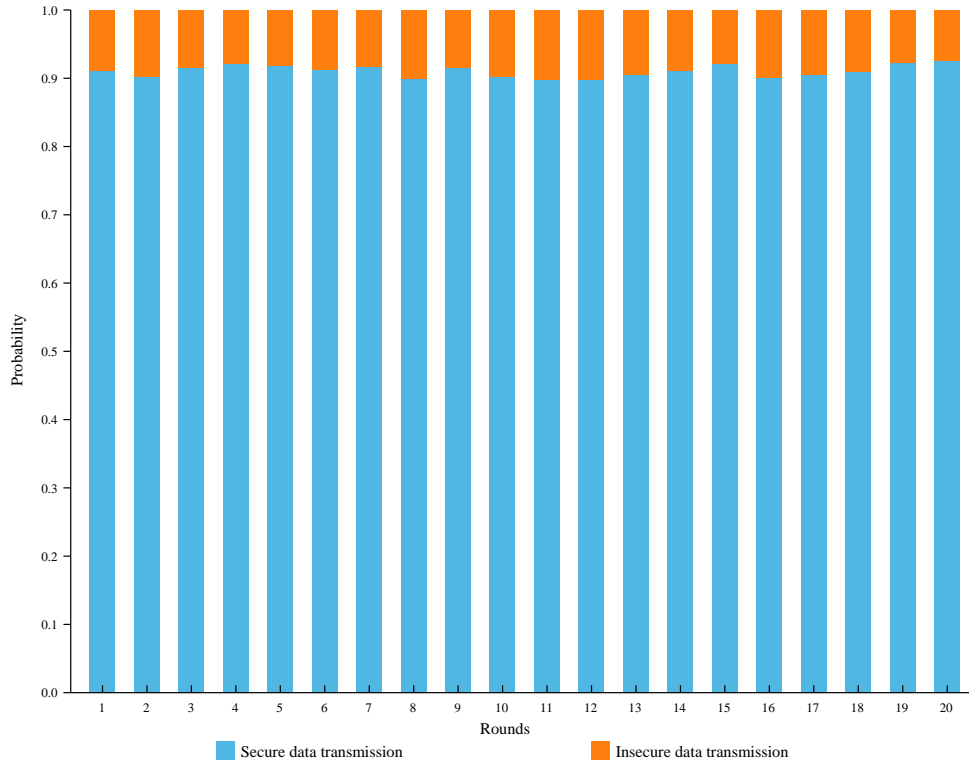


Supplementary Figure 16: PFC code structure for Application 3. SCL, SRL, and SAL represent secondary controller layer, signal relay layer, and sampling and actuator layer. controller.





Supplementary Figure 18: Comparison of the performance metrics of the microgrid system under different centralized approaches: (a) the security performance index  $H_{\alpha,pfc}$ , (b) the control performance index  $J_{task,pfc}$ . The middle part of the figure shows two enlarged subplots. The method labeled as ‘Existing method’ corresponds to the approach in [58] of the paper (Application 3).



Supplementary Figure 19: Ratio of probability of successful defense w.r.t. probability of unsuccessful defense for DC microgrids under PFC-based secondary control over 20 independent repeated trials (Application 3).

---

**Supplementary Algorithm 1** Performance validation on the actuator in UPoT.

---

**Require:** The two kind of values  $u_{i,1}^*(t)$  and  $u_{i,2}^*(t)$  arriving at the actuator, their respective quantities  $Num_{u1}$  and  $Num_{u2}$ , and threshold  $\tilde{\alpha}$  ( $\tilde{\alpha} \in [0, 0.5]$ ) for triggering performance comparison

- 1: **Initialization:** Let  $t = 0$
- 2: **while** UPoT is activated **do**
- 3:   Define a ratio  $\alpha = Num_{u1}/(Num_{u1} + Num_{u2})$
- 4:   **If**  $\alpha \in [\tilde{\alpha}, 1 - \tilde{\alpha}]$  **then**
- 5:     Calculate the PIF  $J_1 = \text{cost}(u_{i,1}^*(t), \cdot)$
- 6:     Calculate the PIF  $J_2 = \text{cost}(u_{i,2}^*(t), \cdot)$
- 7:     **If**  $J_1 < J_2$  **then**
- 8:       Update  $u_{i,PoT}^*(t) = u_{i,1}^*(t)$
- 9:     **else**
- 10:      Update  $u_{i,PoT}^*(t) = u_{i,2}^*(t)$
- 11:     **end if**
- 12:   **else**
- 13:     **If**  $Num_{u1} > Num_{u2}$  **then**
- 14:      Update  $u_{i,PoT}^*(t) = u_{i,1}^*(t)$
- 15:     **else**
- 16:      Update  $u_{i,PoT}^*(t) = u_{i,2}^*(t)$
- 17:     **end if**
- 18:   **end if**
- 19:   Return  $u_{i,PoT}^*(t)$
- 20:   Let  $t \leftarrow t + 1$
- 21: **end while**

where  $\text{cost}(u, \cdot)$  represents the cost function related to control performance as the system evolves according to the control input  $u$ .

---



---

**Supplementary Algorithm 2** Activation strategy acquisition for blockchain nodes based on a stochastic game

---

- Require:** System dynamics, one-stage performance metric (reward function) and game settings
- 1: **Initialization:** Initialize the Q-matrix, activation strategy, and attack strategy
  - 2: **while** Q-matrix has not reached the stability threshold **do**
  - 3:   Both the blockchain and the attacker select their respective actions based on the current strategy
  - 4:   Observe the evolution of the system and calculate the reward at this stage
  - 5:   Update the Q-matrix according to the Bellman equation
  - 6:   Solve the max-min optimization problem using the current Q-matrix to obtain new optimal strategies and game profits for both the blockchain and the attacker
  - 7: **end while**
  - 8: Return the optimal activation strategy for the blockchain nodes
-



### III. SUPPLEMENTARY TABLES

Supplementary Table 1: Characteristics of extensions of PoT

Extensions	C1	C2	C3	C4	VPC*	Security	Computational demand	Complexity
UPoT	Yes	Yes	Yes	Yes	+	$\approx 2$ times PoT	$\approx$ PoT	$\geq$ PoT
DPoT	–	Yes	–	–	\	$\leq$ PoT	$\leq$ PoT	$\leq$ PoT
PoT	Yes	Yes	Yes	Yes	\	Benchmark		

C1, C2, C3 and C4 are the blockchain elements described in the text. VPC\* indicates that validation and performance comparisons are executed on the actuator side. + and – respectively express the operations of deleting and adding blockchain elements.

Supplementary Table 2: Meaning of the fifteen variables presented in Fig. 5 of the main text

Affiliated	Legend	Meaning
DGU 1	$u_1$	Control command
	$x_{12}$	State sent by DGU 2
	$x_{15}$	State sent by DGU 5
DGU 2	$u_2$	Control command
	$x_{23}$	State sent by DGU 3
	$x_{21}$	State sent by DGU 1
DGU 3	$u_3$	Control command
	$x_{34}$	State sent by DGU 4
	$x_{32}$	State sent by DGU 2
DGU 4	$u_4$	Control command
	$x_{43}$	State sent by DGU 3
	$x_{45}$	State sent by DGU 5
DGU 5	$u_5$	Control command
	$x_{51}$	State sent by DGU 1
	$x_{54}$	State sent by DGU 4

Supplementary Table 3: Probability of secure data transmission in the multi-area power system with different approaches

Methods\Areas	Area 1	Area 2	Area 3
Method 1*	0.54	0.57	0.61
Method 2*	<b>0.96</b>	<b>0.93</b>	<b>0.97</b>

Method 1\* and Method 2\* refer to the approach proposed in [57] and the PoT-based LFC method in this paper, respectively.

Supplementary Table 4: Probability of secure data transmission in the DC microgrid system with different approaches

Methods\DGUs	DGU 1	DGU 2	DGU 3	DGU 4	DGU 5
Method 1*	0.48	0.47	0.47	0.48	0.51
Method 2*	<b>0.90</b>	<b>0.91</b>	<b>0.91</b>	<b>0.92</b>	<b>0.92</b>

Method 1\* and Method 2\* refer to the approach proposed in [58] and the PFC-based secondary control in this paper, respectively.

Supplementary Table 5: Details of the software in the blockchain platform

Software	Version
Geth	1.9.10
Remix	0.91
Solidity	8.10.0
Web3.py	5.12.0
Raspberry Pi	0.91
VNC Viewer	0.91
Python	3.92

Supplementary Table 6: Details of solvers used in the experiments

Solver	Version
CPLEX	12.10.0
GUROBI	10.0.3
XPRESS	9.4.0
COPT	7.1.3
MOSEK	10.2.0

Supplementary Table 7: Meaning of seven legends shown in Supplementary Figure 7

Legend	Meaning	
	Solver name	Solver setting
Sol-1	CPLEX	Default
Sol-2	CPLEX	Barrier.convergetol = $1e - 3$
Sol-3	GUROBI	Default
Sol-4	XPRESS	Default
Sol-5	CPLEX	Barrier.convergetol = $1e - 9$
Sol-6	COPT	Default
Sol-7	MOSEK	Default

Supplementary Table 8: Score flags and their meanings for peers with a solver

Score flag of a peer with a specific solver	Meaning		
	Being selected in a delegation	Solution satisfying the constraints	Solution winning consensus
0	×	\	\
-1	✓	×	\
1	✓	✓	×
2	✓	✓	✓

✓ means 'Yes'.

×

\ means 'Not applicable'.

#### IV. SUPPLEMENTARY NOTE 1: PRELIMINARIES FOR BLOCKCHAIN

A P2P network consisting of multiple nodes provides the physical foundation for blockchain [1]. The consensus mechanism, which specifies the criteria for nodes on a P2P network to reach agreement on data, is the core of blockchain [2]. The smart contract, on the other hand, automatically executes the actions including transferring funds to the relevant parties and updates the state of each node after consensus is achieved [3].

## V. SUPPLEMENTARY NOTE 2: SEARCHING AND VERIFYING SOLUTIONS TO A REGULATION PROBLEM

Since actual large-scale renewable energy power systems are usually physically coupled [4], [5], they can be represented as linear multi-agent systems with state coupling as follows

$$\dot{x}_i(t) = A_{ii}x_i(t) + B_i u_i(t) + \sum_{j \in \mathcal{N}_i^p} A_{ij}x_j(t) \quad (1)$$

where  $A_{ii}$ ,  $B_i$  and  $A_{ij}$  are system matrices,  $x_i$  is the state of the  $i$ th subsystem, and  $\mathcal{N}_i^p$  is the set consisting of subsystems physically connected to the  $i$ th one. It should be noted that if the renewable energy power system contains nonlinear components, such as constant power loads, the obtained original nonlinear model can be transformed into the form of (1) by the fully actuated system approach [6].

In real-time optimal control scenarios, information from neighbors is often not communicated in a timely manner due to a variety of reasons, such as the presence of time delays and the optimization of future trajectories. In this regard, it is assumed that the available information of neighbors is  $\tilde{x}_j$ . Utilizing  $\tilde{x}_j$ , the system equation (1) can be rewritten as a model with noise

$$\begin{aligned} x_i(k+1) &= A_{ii}x_i(k) + B_i u_i(k) + \sum_{j \in \mathcal{N}_i^p} A_{ij}(\tilde{x}_j(k) + (x_j(k) - \tilde{x}_j(k))) \\ &= A_{ii}x_i(k) + B_i u_i(k) + \sum_{j \in \mathcal{N}_i^p} A_{ij}\tilde{x}_j(k) + \omega_i(k) \end{aligned} \quad (2)$$

where  $\omega_i(k) = \sum_{j \in \mathcal{N}_i^p} A_{ij}(x_j(k) - \tilde{x}_j(k))$ . Based on the characteristics of distributed control, the following nominal model can be obtained

$$\hat{x}_i(k+1) = A_{ii}\hat{x}_i(k) + B_i \hat{u}_i(k) + \sum_{j \in \mathcal{N}_i^p} A_{ij}\tilde{x}_j(k). \quad (3)$$

According to the regulation task of the renewable energy power system, the control objective function can be described as

$$J_i(\hat{x}_i(k), \hat{u}_i(k : k+T-1)) = \sum_{l=0}^{T-1} J_i^S(\hat{x}_i(k+l), \hat{u}_i(k+l)) + J_i^F(\hat{x}_i(k+T)) \quad (4)$$

where  $T$  is a finite prediction horizon,  $J_i^S(\hat{x}_i(k+l), \hat{u}_i(k+l))$  and  $J_i^F(\hat{x}_i(k+T))$  are referred to as the stage cost function and the terminal cost function, respectively. In this way, the optimization problem issued to the blockchain network can be given as

$$\min_{\hat{x}_i(k), \hat{u}_i(k:k+T-1)} J_i(\hat{x}_i(k), \hat{u}_i(k : k+T-1)) \quad (5)$$

s.t.,

$$\hat{x}_i(k+l+1) = A_{ii}\hat{x}_i(k+l) + B_i \hat{u}_i(k+l) + \sum_{j \in \mathcal{N}_i^p} A_{ij}\tilde{x}_j(k+l) \quad (6a)$$

$$x_i(k) - \hat{x}_i(k) \in \mathbb{Z}_i \quad (6b)$$

$$\hat{x}_i(k+l) - \tilde{x}_i(k+l) \in \mathbb{E}_i \quad (6c)$$

$$\hat{x}_i(k+l) \in \hat{\mathbb{X}}_i \quad (6d)$$

$$\hat{u}_i(k+l) \in \hat{\mathbb{U}}_i \quad (6e)$$

$$\hat{x}_i(k+T) \in \hat{\mathbb{X}}_i^F \quad (6f)$$

for  $l = 0, 1, \dots, T-1$ , where  $\mathbb{Z}_i$ ,  $\mathbb{E}_i$ ,  $\hat{\mathbb{X}}_i$ ,  $\hat{\mathbb{U}}_i$ , and  $\hat{\mathbb{X}}_i^F$  denote the robust invariant set, the set of prediction bias constraints, the set of nominal state constraints, the set of nominal control signal constraints, and the set of terminal constraints of the nominal system, respectively. It is worth mentioning that more constraints can be imposed depending on the actual regulation task.

The above optimization problem will be released to all blockchain nodes. Then, each blockchain node will choose an appropriate solver to address the above optimization problem according to its own computational resources. Eventually, the relative best value of this optimization problem can be obtained in the blockchain belonging to the  $i$ th subsystem

as  $\hat{u}_i(k+l), \hat{x}_i(k+l)$  for  $l = 0, 1, \dots, T-1$ . As a result, the actual control input to the system can be designed as

$$u_i(k) = \hat{u}_i(k + \tau_i) + K_i^{aux}(x_i(k) - \hat{x}_i(k)) \quad (7)$$

and the data used to communicate with the neighbors is given as

$$\tilde{x}_i(k+T) = \hat{x}_i(k+T) \quad (8)$$

where  $\tau_i$  ( $\tau_i \leq T$ ) is the latency induced by PoT,  $K_i^{aux}$  is the control gain. Notice that  $\hat{u}_i(k + \tau_i)$  is not only an optimal control, but also a predictive control that can compensate for the delay brought about by PoT. State prediction is an effective solution for actively compensating for communication-induced delays in networked control systems [7]. The above designs give the PoT consensus mechanism both security and real-time nature, where security is inherited from verification and real-time nature is endowed by state prediction.

Up to this point, if the communication is free from attacks and the blockchain nodes are honest, then the control that makes the system stable and optimal can be obtained by choosing the appropriate constraint set as well as solver for the optimization problem.

It should be pointed out that it is not possible to accurately look longitudinally at the evolutionary trajectory of the coupled system over its entire life cycle at each transient time slice of each distributed unit. Accordingly, it is difficult to ensure the stability of a system over its entire life cycle by validating conditions in stages. Whereas the combination of constraints (6a)-(6f) provides a valuable, interoperable, and practical verification criterion for the stability of the system, which overcomes the above-mentioned difficulty. Specifically, when each blockchain node receives candidate solutions, they will first verify whether these solutions satisfy conditions (6a)-(6f). The careful selection of the constraint set will reflect the requirements for system stability. Therefore, all solutions satisfying conditions (6a)-(6f) will form a subset of all feasible solutions capable of stabilizing the system [8]. In other words, the solution satisfies the stability requirements of the system as long as it is verified to satisfy conditions (6a)-(6f). It can be seen that the proposed verification mechanism embedded in PoT meets the system requirements for stability. It is also worth mentioning that the mechanism gives PoT the characteristics of what an excellent consensus protocol should have. That is, it is difficult to find a solution to the optimal problem in PoT, while it is easy to verify whether it satisfies the requirements. Further, a relatively optimal solution can be found among the set of feasible solutions that have passed this verification process based on the performance metric function. At this point, the verification of the optimal solution to the regulation problem is completed.

## VI. SUPPLEMENTARY NOTE 3: POT-BASED DISTRIBUTED SECONDARY REGULATION STRATEGY

### A. Abbreviation

MG	Microgrid
DGUs	Distributed generation units
PCCs	Point of common couplings
KVL	Kirchhoff's voltage law
KCL	Kirchhoff's current law
AVR	Average voltage recovery
PCS	Proportional current sharing

### B. Variable and Parameter

$V_i$	Output voltage of $i$ th DGU
$I_{ti}$	Inductance current of $i$ th DGU
$I_{ik}$	Current on tie line $ik$
$V_{in,i}$	Input voltage of $i$ th DGU
$d_{c,i}$	Duty cycle of $i$ th DGU
$R_{ti}, L_{ti}, C_{ti}$	Filter resistance, filter inductance and shunt capacitor of $i$ th DGU
$R_{Li}$	Local load resistance of $i$ th DGU
$R_{ik}$	Power line resistance between $i$ th and $k$ th DGU
$L_{ik}$	Power line inductance between $i$ th and $k$ th DGU
$\theta_i^s$	Proportional factor for current sharing of $i$ th DGU
$V^{ref}$	Desired voltage value
$\bar{V}_i$	Estimate of the output voltage $V_i$
$\delta_i$	Correction term in the droop control of $i$ th DGU
$R_{vi}$	Droop factor of $i$ th DGU
$v_{o,i}^*$	Voltage reference for inner control loop of $i$ th DGU
$K_{pvi}, K_{ivi}$	PI gains for the voltage loop of $i$ th DGU
$K_{pci}, K_{ici}$	PI gains for the current loop of $i$ th DGU
$\mathcal{N}_i^e, \mathcal{N}_i^c$	Sets of neighboring DGUs of $i$ th DGU respectively on the physical and information layers
$N$	The total number of DGUs in the MG system

### C. System Model of DC Microgrids

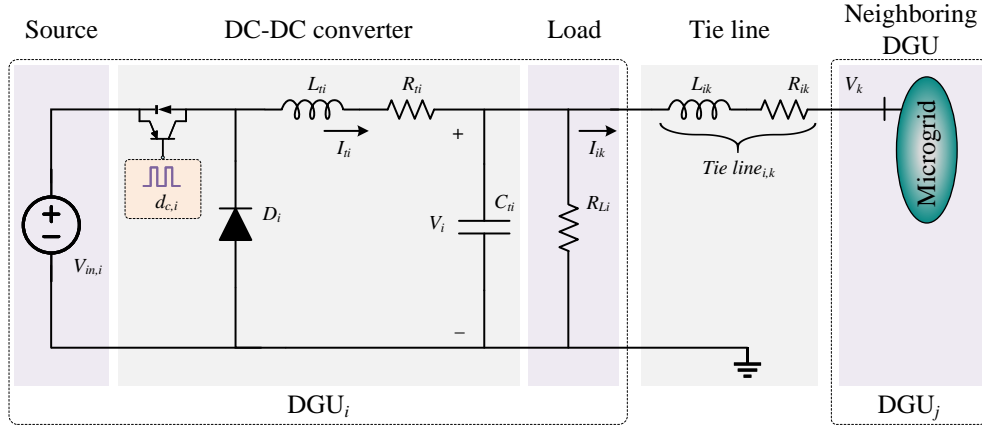
This part presents the model of the islanded DC microgrid illustrated in Supplementary Figure 20. Notice that using the Y- $\Delta$  transform for the IEEE 9-bus circuit shown in Supplementary Figure 4 gives the system in Supplementary Figure 20 and yields  $R_{ik}$  [9]. The intermittent nature of wind and solar power is a major factor in reducing the quality of power supply. To this end, it is assumed here that the energy storage scheme solves the fluctuation problem of renewable energy well. According to KVL and KCL, the dynamics of the DGU  $i$  based on the converter interface can be described as follows

$$\begin{aligned}
 \dot{V}_i(t) &= \frac{I_{ti}(t)}{C_{ti}} + \frac{1}{C_{ti}} \sum_{k \in \mathcal{N}_i^e} I_{ik}(t) - \frac{V_i(t)}{C_{ti}R_{Li}} \\
 \dot{I}_{ti}(t) &= -\frac{V_i(t)}{L_{ti}} - \frac{R_{ti}}{L_{ti}} I_{ti}(t) + \frac{V_{in,i}d_{c,i}(t)}{L_{ti}} \\
 \dot{I}_{ik}(t) &= -\frac{R_{ik}}{L_{ik}} I_{ik}(t) + \frac{V_k(t) - V_i(t)}{L_{ik}}
 \end{aligned} \tag{9}$$

$\forall i \in \{1, \dots, N\}, k \in \mathcal{N}_i^e = \{1, \dots, N_{i,m}\}$ , where  $N_{i,m}$  is the number of transmission lines connected to DGU  $i$ .

It is assumed that the coupling line is resistive dominated [10], i.e.,  $dI_{ik}(t)/dt = 0, k \in \mathcal{N}_i^e$ . In this way, the dynamics of the tie line in (9) can be given as

$$I_{ik}(t) = \frac{1}{R_{ik}}(V_k(t) - V_i(t)), k \in \mathcal{N}_i^e. \tag{10}$$



Supplementary Figure 20: Equivalent circuit diagram of a microgrid with a meshed topology.

Substituting (10) into (9) yields the dynamics of the DGU  $i$  as follows

$$\begin{aligned} \dot{V}_i(t) &= \frac{I_{ti}(t)}{C_{ti}} + \sum_{k \in \mathcal{N}_i^e} \frac{V_k(t) - V_i(t)}{C_{ti}R_{ik}} - \frac{V_i(t)}{C_{ti}R_{Li}} \\ \dot{I}_{ti}(t) &= -\frac{V_i(t)}{L_{ti}} - \frac{R_{ti}}{L_{ti}}I_{ti}(t) + \frac{V_{in,i}d_{r,i}(t)}{L_{ti}}. \end{aligned} \quad (11)$$

#### D. Regulation Objectives of DC microgrids

In the secondary control of a DC MG, one of the main control objectives is to share the total load demand between DGUs at steady state in proportion to the rated current of the DGUs [11], i.e.,

$$\lim_{t \rightarrow \infty} \left\| \frac{I_{tj}(t)}{\theta_j^s} - \frac{I_{ti}(t)}{\theta_i^s} \right\| = 0 \quad (12)$$

for  $i, j \in \{1, \dots, N\}$ , where  $\theta_i^s$  is the expected current sharing ratio related to the rated current of the  $i$ th DGU.

In addition, another regulation target is to restore the weighted average value of the voltage signals at the PCCs to  $V^{ref}$  at steady state [12], i.e.,

$$\lim_{t \rightarrow \infty} \frac{1}{N} \sum_{i=1}^N \|V_i(t) - V^{ref}\| = 0. \quad (13)$$

It should be noted that the reference voltage  $V^{ref}$  in (13) is generated by the upper control layer (i.e., the tertiary control layer) and can only be accessed by a portion of the generation units.

#### E. Dynamics of Multi-Bus DC Microgrids

In this paper, the commonly used hierarchical control structure is taken into account. Since hierarchical control contains other dynamics, such as those of the inner control loops, (11) does not fully describe the dynamics of the microgrid system. To this end, the characteristics of the individual control loops need to be modeled in addition to the description of the underlying circuit model.

First, nearest to the power electronics is the inner control loop, which realizes the tracking of the primary reference input through the duty cycle adjustment. Usually the inner control is structured as a double closed loop in the following form

$$\begin{aligned} i_{i_i}^*(t) &= K_{pvi}(v_{o,i}^*(t) - v_{o,i}(t)) + K_{ivi} \int (v_{o,i}^*(\tau) - V_i(\tau)) d\tau \\ d_{c,i}(t) &= K_{pci}(i_{i_i}^*(t) - i_{i_i}(t)) + K_{ici} \int (i_{i_i}^*(\tau) - i_{i_i}(\tau)) d\tau \end{aligned} \quad (14)$$



where  $v_{o,i}^*(t)$  is the reference input given into the inner control loop,  $K_{pvi}$  and  $K_{ivi}$  are the PI control parameters for the voltage outer loop,  $K_{pci}$  and  $K_{ici}$  are the PI control parameters for the current inner loop. It can be seen that there are two integral links contained in the inner loop control loop, i.e.,

$$\begin{aligned}\dot{\phi}_i(t) &= v_{o,i}^*(t) - v_{o,i}(t) \\ \dot{\gamma}_i(t) &= i_{li}^*(t) - i_{li}(t)\end{aligned}\quad (15)$$

where  $\phi_i$  is called the integral variable of the voltage outer loop,  $\gamma_i(t)$  is the integral variable of the current inner loop. The feedback signals  $v_{o,i}(t)$  and  $i_{li}(t)$  in the inner loops are chosen as  $V_i(t)$  and  $I_{ti}(t)$ , respectively. Substituting (15) into (14), the inner loop control loop can be rewritten as

$$\begin{aligned}i_{li}^*(t) &= K_{pvi}(v_{o,i}^*(t) - V_i(t)) + K_{ivi}\phi_i(t) \\ d_{c,i}(t) &= K_{pci}(i_{li}^*(t) - I_{ti}(t)) + K_{ici}\gamma_i(t).\end{aligned}\quad (16)$$

In general, droop control is used as an interface to enable the interaction of the device layer with the upper control layer, as well as to roughly realize the power equalization at the time of grid-connection. Such an approach is also considered in this paper and the droop control is given as follows

$$v_{o,i}^*(t) = V_{ni} - R_{vi}I_{ti}(t) + \delta_i(t)\quad (17)$$

where  $V_{ni}$  is the nominal voltage value,  $R_{vi}$  is the droop factor, and  $\delta_i(t)$  is the correction term. It is worth mentioning that the correction term  $\delta_i(t)$  is also referred to as the secondary control input to be designed towards various regulation goals.

Considering the contradiction between consistent voltage recovery and current balancing, it is also necessary to design the following voltage estimator to accomplish the goal of global AVR given in (13)

$$\bar{V}_i(t) = V_i(t) + k_i \int \sum_{j \in \mathcal{N}_i^e} a_{ij}(\bar{V}_j(\tau) - \bar{V}_i(\tau))d\tau\quad (18)$$

where  $\bar{V}_i$  and  $\bar{V}_j$  are respectively the estimates of the output voltages  $V_i$  and  $V_j$ ,  $k_i$  is the coupling gain for this estimator.

In this way, the duty cycle  $d_{c,i}$  of the inner control loop can be calculated as

$$\begin{aligned}d_{c,i}(t) &= K_{pci}K_{pvi}V_{ni} - K_{pci}\check{R}_{vi}I_{ti}(t) + K_{pci}K_{pvi}\delta_i(t) \\ &\quad - K_{pci}K_{pvi}V_i(t) + K_{pci}K_{ivi}\phi_i(t) + K_{ici}\gamma_i(t)\end{aligned}\quad (19)$$

where  $\check{R}_{vi} = K_{pvi}R_{vi} + 1$ . Up to this point, the description of each part of the microgrid under hierarchical control is presented.

To obtain a large signal model of the microgrid system, the state variable is taken to be  $x_i(t) = [V_i(t), I_{ti}(t), \phi_i(t), \gamma_i(t), \bar{V}_i(t)]^T$  and the control input is selected as  $u_i(t) = \delta_i(t)$ . Regarding (11), (15), (18) and (19), the dynamical behavior of the considered multi-bus DC microgrid can be characterized by the following model

$$\dot{x}_i(t) = A_{ii}^{[mg,c]}x_i(t) + \sum_{k \in \mathcal{N}_i^e} A_{ik}x_k(t) + B_i^{[mg,c]}u_i(t) + D_i^{[mg,c]}V_{ni}\quad (20)$$

where  $\eta_i = (R_{Li}^{-1} + d_{i,R}^{in})$ ,  $d_{i,R}^{in} = \sum_{j \in \mathcal{N}_i^e} R_{ij}^{-1}$ ,  $d_i^{in} = \sum_{j \in \mathcal{N}_i^e} a_{ij}$ ,  $D_i^{[mg,c]} = [0 \ V_{in,i}K_{pci}K_{pvi}/L_{ti} \ 1 \ K_{pvi} \ 0]^T$ ,

$$A_{ii}^{[mg,c]} = \begin{bmatrix} -\frac{\eta_i}{C_{ti}} & \frac{1}{C_{ti}} & 0 & 0 & 0 \\ -\frac{1+V_{in,i}K_{pci}K_{pvi}}{L_{ti}} & -\frac{R_{ti}+V_{in,i}K_{pci}\check{R}_{vi}}{L_{ti}} & \frac{V_{in,i}K_{pci}K_{ivi}}{L_{ti}} & \frac{V_{in,i}K_{ici}}{L_{ti}} & 0 \\ -1 & -R_{vi} & 0 & 0 & 0 \\ -K_{pvi} & -K_{pvi}R_{vi} & K_{ivi} & 0 & 0 \\ -\frac{\eta_i}{C_{ti}} & \frac{1}{C_{ti}} & 0 & 0 & 0 \end{bmatrix}$$

$$A_{ij}^{[mg,c]} = \begin{bmatrix} 0 & 0 & 0 & 0 & 0 \\ 0 & 0 & 0 & 0 & 0 \\ 0 & 0 & 0 & 0 & 0 \\ 0 & 0 & 0 & 0 & 0 \\ -k_i d_{i,R}^{in} & k_i a_{ij} & 0 & 0 & 0 \end{bmatrix}, \quad B_i^{[mg,c]} = \begin{bmatrix} 0 \\ L_{ti}^{-1}V_{in,i}K_{pci}K_{pvi} \\ 1 \\ K_{pvi} \\ 0 \end{bmatrix}.$$

### F. PoT-Based Secondary Regulation Strategy

Discretizing (20) at the sampling period  $T_s$  yields

$$\begin{aligned}
V_i(k+1) &= V_i(k) + T_c \frac{I_{ti}(k)}{C_{ti}} + T_c \sum_{j \in \mathcal{N}_i^e} a_{ij} \frac{V_j(k) - V_i(k)}{C_{ti} R_{ij}} - T_c \frac{V_i(k)}{C_{ti} R_{Li}} \\
I_{ti}(k+1) &= I_{ti}(k) - T_c \frac{V_i(k)}{L_{ti}} - T_c \frac{R_{ti}}{L_{ti}} I_{ti}(k) + T_c \frac{V_i^{in} d_{c,i}(k)}{L_{ti}} \\
\phi_i(k+1) &= \phi_i(k) + T_c V_{ni}^* - T_c R_{vi} I_{ti}(k) + T_c \delta_i(k) - T_c V_i(k) \\
\gamma_i(k+1) &= \gamma_i(k) + K_{pvi} V_{ni}^{ref} - K_{pvi} R_{vi} I_{ti}(k) + K_{pvi} \delta_i(k) - K_{pvi} V_i(k) + K_{ivi} \phi_i(k) \\
\bar{V}_i(k+1) &= \bar{V}_i(k) + \Delta V_i(k+1) + T_c K_i^{obs} \sum_{j \in \mathcal{N}_i^e} a_{ij} (\bar{V}_j(k) - \bar{V}_i(k))
\end{aligned} \tag{21}$$

where  $\Delta$  is the incremental operator, i.e.,  $\Delta V_i(k+1) = V_i(k+1) - V_i(k)$ . This operator has the same meaning later and will not be repeated.

Recalling the regulation objectives of AVR and PCS, define the tracking error of the observed voltage as

$$e_i^V(k) = V^{ref} - \bar{V}_i(k) \tag{22}$$

as well as the cooperation error of the current as

$$\varepsilon_i^I(k) = \sum_{j \in \mathcal{N}_i^e} a_{ij} \left( \frac{I_{tj}(k-1)}{\theta_j^s} - \frac{I_{ti}(k-1)}{\theta_i^s} \right). \tag{23}$$

Incorporating (21)-(23), the augmented microgrid system in incremental form can be obtained as follows

$$\begin{aligned}
\Delta V_i(k+1) &= \left(1 - \frac{T_c \eta_i}{C_{ti}}\right) \Delta V_i(k) + \frac{T_c}{C_{ti}} \Delta I_{ti}(k) + \sum_{j \in \mathcal{N}_i^e} \frac{T_c}{C_{ti} R_{ij}} \Delta V_j(k) \\
\Delta I_{ti}(k+1) &= -\frac{T_c(1 + V_{in} K_{pci} K_{pvi})}{L_{ti}} \Delta V_i(k) + \left(1 - \frac{T_c(R_{ti} + V_{in} K_{pci} \check{R}_{vi})}{L_{ti}}\right) \Delta I_{ti}(k) \\
&\quad + \frac{T_c V_{in} K_{pci} K_{ivi}}{L_{ti}} \Delta \phi_i(k) + \frac{T_c V_{in} K_{ici}}{L_{ti}} \Delta \gamma_i(k) + \frac{T_c V_{in} K_{pci} K_{pvi}}{L_{ti}} \Delta \delta_i(k) \\
\Delta \phi_i(k+1) &= -T_c \Delta V_i(k) - T_c R_{vi} \Delta I_{ti}(k) + \Delta \phi_i(k) + T_c \Delta \delta_i(k) \\
\Delta \gamma_i(k+1) &= \Delta \gamma_i(k) - T_c (K_{pvi} R_{vi} + 1) \Delta I_{ti}(k) + T_c K_{pvi} \Delta \delta_i(k) - T_c K_{pvi} \Delta V_i(k) + T_c K_{ivi} \Delta \phi_i(k) \\
e_i^V(k+1) &= (1 - T_c K_i^{obs} d_i^{in}) \Delta e_i^V(k) + \left(T_c \frac{\eta_i}{C_{ti}} - 1\right) \Delta V_i(k) - T_c \frac{1}{C_{ti}} \Delta I_{ti}(k) \\
&\quad - T_c \sum_{j \in \mathcal{N}_i^e} \frac{1}{C_{ti} R_{ij}} \Delta V_j(k) + T_c K_i^{obs} \sum_{j \in \mathcal{N}_i^e} a_{ij} e_j^V(k) \\
\varepsilon_i^I(k+1) &= \varepsilon_i^I(k) - \frac{d_i^{in}}{\theta_i^s} \Delta I_{ti}(k) + \sum_{j \in \mathcal{N}_i^e} \frac{a_{ij}}{\theta_j^s} \Delta I_{tj}(k).
\end{aligned} \tag{24}$$

Further, take  $x_i(k) = [\Delta V_i(k), \Delta I_{ti}(k), \Delta \phi_i(k), \Delta \gamma_i(k), e_i^V(k), \varepsilon_i^I(k)]^T$ ,  $u_i(k) = \Delta \delta_i(k)$ . The above system can be represented in a compact form as follows

$$x_i(k+1) = A_{ii}^{[mg,d]} x_i(k) + B_i^{[mg,d]} u_i(k) + \sum_{j \in \mathcal{N}_i^e} A_{ij}^{[mg,d]} x_j(k) \tag{25}$$

where  $A_{ii}^{[mg,d]}$ ,  $B_i^{[mg,d]}$  and  $A_{ij}^{[mg,d]}$  can be obtained from (24). It can be seen that the regulation task given in (12) and (13) can be accomplished and the stable operation of the microgrid can be ensured if the designed secondary control can make the state of the system (25) converge to the origin. Up to this point, we get a system model like (2).

Next, based on the secondary regulation tasks (12) and (13) of the DC microgrid, the following control cost function can be designed

$$J_i(\hat{x}_i(k), \hat{u}_i(k : k+T-1)) = \sum_{l=0}^{T-1} J_i^S(\hat{x}_i(k+l), \hat{u}_i(k+l)) + J_i^F(\hat{x}_i(k+T)) \tag{26}$$

where  $T$  is a finite prediction horizon, and

$$\begin{aligned} J_i^S(\hat{x}_i(k), \hat{u}_i(k)) &= \|\hat{x}_i(k)\|_{Q_i}^2 + \|\hat{u}_i(k)\|_{R_i}^2 \\ J_i^F(\hat{x}_i(k)) &= \|\hat{x}_i(k)\|_{P_i}^2 \end{aligned} \quad (27)$$

where  $Q_i$ ,  $R_i$  and  $P_i$  are weight matrices. Following the narrative in Supplementary Note 2 and the aforementioned microgrid system model, each blockchain node would solve the following optimization problem corresponding to the microgrid secondary control

$$\min_{\hat{x}_i(k), \hat{u}_i(k:k+T-1)} J_i(\hat{x}_i(k), \hat{u}_i(k:k+T-1)) \quad (28)$$

s.t.,

$$\begin{aligned} \hat{x}_i(k+l+1) &= A_i^{[mg,d]} \hat{x}_i(k+l) + B_i^{[mg,d]} \hat{u}_i(k+l) + \sum_{j \in \mathcal{N}_i^e} A_{ij}^{[mg,d]} \tilde{x}_j(k+l) \\ x_i(k) - \hat{x}_i(k) &\in \mathbb{Z}_i \\ \hat{x}_i(k+l) - \tilde{x}_i(k+l) &\in \mathbb{E}_i \\ \hat{x}_i(k+l) &\in \hat{\mathbb{X}}_i \\ \hat{u}_i(k+l) &\in \hat{\mathbb{U}}_i \\ \hat{x}_i(k+T) &\in \hat{\mathbb{X}}_i^F \end{aligned} \quad (29)$$

for  $l = 0, 1, \dots, T-1$ , where  $\mathbb{Z}_i$ ,  $\mathbb{E}_i$ ,  $\hat{\mathbb{X}}_i$ ,  $\hat{\mathbb{U}}_i$ , and  $\hat{\mathbb{X}}_i^F$  denote the robust invariant set, the set of prediction bias constraints, the set of state constraints, the set of control signal constraints, and the set of terminal constraints of the system, respectively.

Ideally, each blockchain node can obtain the optimal secondary control  $\hat{u}_i(k+l)$  and the optimal predicted state  $\hat{x}_i(k+l)$ . Let  $\tilde{x}_i(k+T) = \hat{x}_i(k+T)$ , then  $\tilde{x}_i(k+T)$  will be sent to the neighboring power generation units. Therefore, the control input  $u_i(k) = \hat{u}_i(k) + K_i^{aux}(x_i(k) - \hat{x}_i(k))$  is available. At this point, step 4 in Fig. 1 is completed. Then, each blockchain node will broadcast the obtained value to others. Further, the nodes of the blockchain network will verify all the received candidate solutions. That is, the solutions that do not satisfy the stability conditions are first eliminated, and then the one with the optimal cost function is identified from them. After finishing the above step (i.e., step 5 in Fig. 1), each blockchain node issues the verified optimal solution to the ASDM. Ultimately, the secure and optimal secondary control input for microgrid systems is selected according to the majority rule principle on the ASDM. Then, the actual correction obtained by the  $i$ th DGU is  $\delta_i(k) = \delta_i(k-1) + u_{i, PoT}^*(k)$ .

To reflect the trustworthiness of the data obtained by REPSs under PoT, the security performance metric is set as

$$\begin{aligned} H_\alpha &= \sum_{t=t_{sec}}^{t_{sec}+T} \left( \sum_{i=1}^N \left( \sum_{j \in \mathcal{N}_i^c} \left( \frac{1}{V_{j,max}^{org}} |\tilde{y}_{ij}^V(t) - y_j^{V,org}(t)| + \frac{1}{I_{tj,max}^{org}} |\tilde{y}_{ij}^I(t) - y_j^{I,org}(t)| \right) \right. \right. \\ &\quad \left. \left. + \frac{1}{u_{i,max}^{org}} |\tilde{u}_i(t) - u_i^{org}(t)| \right) \right) \end{aligned} \quad (30)$$

where the meanings of the involved variables are presented in Supplementary Table 9. It should be noted that  $V_{j,max}^{org}$ ,  $I_{tj,max}^{org}$ , and  $u_{i,max}^{org}$  are used for normalization. Similarly, in order to reflect the performance of the control strategy in accomplishing a given control task of the REPSs, the control performance metric is defined as

$$J_{task} = \sum_{t=t_{sec}}^{t_{sec}+T} \sum_{i=1}^N \left( \frac{1}{\bar{V}_{i,max}^{org}} |\bar{V}_i(t) - V^{ref}| + \sum_{j \in \mathcal{N}_i^c} \left( \frac{1}{I_{tj,max}^{org}} \left| \frac{I_{tj}^{org}(t)}{\theta_j^s} - \frac{I_{ti}^{org}(t)}{\theta_i^s} \right| \right) \right) \quad (31)$$

where  $t_{sec}$ ,  $T$  and  $N$  have the same meaning as given in Supplementary Table 9,  $\bar{V}_i(t)$  is presented in (18), variables  $V^{ref}$ ,  $\mathcal{N}_i^c$  and  $\theta_i$  have the same meaning as those in the manuscript, and the meanings of the other variables are available in Supplementary Table 10.

Supplementary Table 9: Meanings of the variables in equation (30)

<b>Variable</b>	<b>Meaning</b>
$t_{sec}$	Moment activating the secondary control strategy
$T$	Action time of the secondary control strategy
$N$	Number of DGUs contained in the microgrid
$y_j^{V,org}(t)$	Ideal voltage value of DGU $j$ in the microgrid
$y_j^{I,org}(t)$	Ideal current value of DGU $j$ in the microgrid
$u_i^{org}(t)$	Ideal control command of DGU $i$ in the microgrid
$\tilde{y}_{ij}^I(t)$	Voltage value actually used by the controller in the microgrid, which received by DGU $i$ from DGU $j$
$\tilde{y}_{ij}^V(t)$	Current value actually used by the controller in the microgrid, which is received by DGU $i$ from DGU $j$
$\tilde{u}_i(t)$	Control command actually used by the actuator of DGU $i$ in the microgrid
$V_{j,max}^{org}$	Maximum ideal voltage value of DGU $j$ during secondary control period
$I_{tj,max}^{org}$	Maximum ideal current value of DGU $j$ during secondary control period
$u_{i,max}^{org}$	Maximum ideal control command of DGU $i$ during secondary control period

Supplementary Table 10: Meanings of the variables in equation (31)

<b>Variable</b>	<b>Meaning</b>
$\bar{V}_{i,max}^{org}$	Maximum ideal estimated voltage value of DGU $i$ during secondary control period
$I_{tj,max}^{org}$	Maximum ideal current value of DGU $j$ during secondary control period
$I_{tj}^{org}(t)$	Ideal/measured current value of DGU $j$ in the microgrid

## VII. SUPPLEMENTARY NOTE 4: POT-BASED DISTRIBUTED LOAD FREQUENCY CONTROL STRATEGY

### A. Abbreviation

LFC	Load frequency control
ACE	Area control error
GRC	Generation rate constraint

### B. Variable and Parameter

$N$	The total number of areas in the power system
$M_i$	Moment of inertia of $i$ th generator
$D_i$	Droop factor of $i$ th generator
$T_{tb,i}$	Time constant of $i$ th the turbine
$T_{g,i}$	Time constant of $i$ th governor
$R_{\omega,i}$	RPM drop
$T_{ij}$	Synchronization factor between area- $i$ and area- $j$
$f_i$	Frequency of area- $i$
$P_{g,i}$	Power of the governor in area- $i$
$P_{mech,i}$	Mechanical power of the turbine in area- $i$
$P_{L,i}$	Load of area- $i$
$P_{tie}^{ij}$	Tie-line power flow between area- $i$ and area- $j$
$P_{tie,i}$	Total tie-line power flow between area- $i$ and its neighbors.
$\Delta x$	Change/deviation of $x$

### C. System Model of Multi-Area Interconnected Power System

For any area- $i$  in the  $N$  power system control areas with aggregated generator units, the overall generator-load dynamics between the incremental mismatch power and the frequency deviation can be given as

$$M_i \Delta \dot{f}_i(t) = \Delta P_{mech,i}(t) - \Delta P_{L,i}(t) - D_i \Delta f_i(t) - \Delta P_{tie,i}(t). \quad (32)$$

The dynamics of the generator can be described as

$$T_{tb,i} \Delta \dot{P}_{mech,i}(t) = \Delta P_{g,i}(t) - \Delta P_{mech,i}(t). \quad (33)$$

The dynamics of the governor can be expressed as

$$T_{g,i} \Delta \dot{P}_{g,i}(t) = \Delta P_{ref,i}(t) - \frac{1}{R_{\omega,i}} \Delta f_i(t) - \Delta P_{g,i}(t) + s_i \Delta P_{e,i}(t) \quad (34)$$

where  $s_i$  is a binary variable and  $s_i = 0$  means that area- $i$  does not contain a wind turbine unit and  $s_i = 1$  denotes that it contains a wind turbine unit. The change in incremental power on the tie line between area- $i$  and area- $j$  is determined by the following equation

$$\Delta \dot{P}_{tie}^{ij}(t) = T_{ij} (\Delta f_i(t) - \Delta f_j(t)). \quad (35)$$

Thus, the dynamics of the incremental power of the total tie line between area- $i$  and the other areas can be given as

$$\Delta \dot{P}_{tie,i}(t) = \sum_{j=1, j \neq i}^N \Delta \dot{P}_{tie}^{ij}(t) = \sum_{j=1, j \neq i}^N T_{ij} (\Delta f_i(t) - \Delta f_j(t)). \quad (36)$$

In summary, (32)-(36) characterize the dynamics of the frequency deviation of a multi-area power system with generator units and wind turbine units [13]. Regulation of multi-area power systems often involves two objectives: stabilizing the frequency and keeping the power interaction between areas stable at a desired value. As a result, for area- $i$ , the commonly used ACE incorporates a frequency deviation and a change in the power of the tie line, i.e.,

$$ACE_i(t) = \beta_i \Delta f_i(t) + \Delta P_{tie,i}(t) \quad (37)$$

where  $\beta_i$  is a coefficient used to balance frequency deviation and power change.

In this way, taking the state variable as  $x_i(t) = [\Delta f_i(t), \Delta P_{mech,i}(t), \Delta P_{g,i}(t), \Delta P_{tie,i}(t)]^T$  and the control input as  $u_i(t) = \Delta P_{ref,i}(t)$ , the frequency response dynamics of this multi-area system can be represented by the interconnected state-space model as follows

$$\begin{aligned} \dot{x}_i(t) &= A_{ii}^{[lfc,c]} x_i(t) + \sum_{j=1}^N A_{ij}^{[lfc,c]} x_j(t) + B_i^{[lfc,c]} u_i(t) + E_i \omega_i(t) \\ y_i(t) &= C_i x_i(t) \end{aligned} \quad (38)$$

where  $\omega_i(t) = [\Delta P_{L,i}(t), \Delta P_{e,i}(t)]$  is the vector of disturbance inputs,  $C_i = [\beta_i, 0, 0, 1]$ ,  $\tilde{T}_i = \sum_{j=1, j \neq i}^N T_{ij}$ ,

$$\begin{aligned} A_{ii}^{[lfc,c]} &= \begin{bmatrix} -\frac{D_i}{M_i} & \frac{1}{M_i} & 0 & -\frac{1}{M_i} \\ 0 & -\frac{1}{T_{tb,i}} & \frac{1}{T_{tb,i}} & 0 \\ -\frac{1}{T_{g,i} R_{\omega,i}} & 0 & -\frac{1}{T_{g,i}} & 0 \\ \tilde{T}_i & 0 & 0 & 0 \end{bmatrix}, A_{ij}^{[lfc,c]} = T_{ij} \begin{bmatrix} 0 & 0 & 0 & 0 \\ 0 & 0 & 0 & 0 \\ 0 & 0 & 0 & 0 \\ -1 & 0 & 0 & 0 \end{bmatrix} \\ E_i &= \begin{bmatrix} -\frac{1}{M_i} & 0 \\ 0 & 0 \\ 0 & \frac{s_i}{T_{g,i}} \\ 0 & 0 \end{bmatrix}, B_i^{[lfc,c]} = \begin{bmatrix} 0 \\ 0 \\ \frac{1}{T_{g,i}} \\ 0 \end{bmatrix}. \end{aligned}$$

#### D. PoT-Based Distributed Load Frequency Control Strategy

Discretization of (38) yields

$$x_i(k+1) = A_{ii}^{[lfc,d]} x_i(k) + B_i^{[lfc,d]} u_i(k) + \sum_{j=1}^N A_{ij}^{[lfc,d]} x_j(k) + E_i^{[lfc,d]} \omega_i(k) \quad (39)$$

where  $T_c$  is the sampling period,  $A_{ii}^{[lfc,d]} = T_c A_{ii}^{[lfc,c]} + I$ ,  $B_i^{[lfc,d]} = T_c B_i^{[lfc,c]}$ ,  $A_{ij}^{[lfc,d]} = T_c A_{ij}^{[lfc,c]}$ , and  $E_i^{[lfc,d]} = T_c E_i^{[lfc,c]}$ .

In a power system, the generation rate of a thermal power unit is subject to constraints, i.e., GRC. Considering the GRC of the generator, the deviation of the generator output power satisfies the following inequality

$$\left| \Delta \dot{P}_{mech,i} \right| = \left| \frac{\Delta P_{g,i} - \Delta P_{mech,i}}{T_{tb,i}} \right| \leq \bar{p}_{mech} \quad (40)$$

where  $\bar{p}_{mech} = 0.0017$  p.u. MW/s is a typical value for GRC [14], [15]. In addition, given the smoothness of the dispatch, the change rate of the load reference point will be limited as follows

$$|\Delta P_{ref,i}| \leq \bar{p}_{ref} \quad (41)$$

where  $\bar{p}_{ref} = 0.3$  is a typical value to be taken.

Based on the objectives of LFC, the following control cost function can be given

$$J_i(\hat{x}_i(k), \hat{u}_i(k : k+T-1)) = \sum_{l=0}^{T-1} J_i^S(\hat{x}_i(k+l), \hat{u}_i(k+l)) + J_i^F(\hat{x}_i(k+T)) \quad (42)$$

where  $T$  is a finite prediction horizon, and

$$\begin{aligned} J_i^S(\hat{x}_i(k), \hat{u}_i(k)) &= \|\hat{x}_i(k)\|_{Q_i}^2 + \|\hat{u}_i(k)\|_{R_i}^2 \\ J_i^F(\hat{x}_i(k)) &= \|\hat{x}_i(k)\|_{P_i}^2 \end{aligned} \quad (43)$$

where  $Q_i$ ,  $R_i$  and  $P_i$  are weight matrices.

Then, the delegates of the blockchain network corresponding to area- $i$  would solve the following optimization problem in a given amount of time

$$\min_{\hat{x}_i(k), \hat{u}_i(k:k+T-1)} J_i(\hat{x}_i(k), \hat{u}_i(k : k+T-1)) \quad (44)$$

s.t.,

$$\begin{aligned}
\hat{x}_i(k+l+1) &= A_i^{[lfc,d]} \hat{x}_i(k+l) + B_i^{[lfc,d]} \hat{u}_i(k+l) + \sum_{\substack{j=1 \\ j \neq i}}^N A_{ij}^{[lfc,d]} \tilde{x}_j(k+l) \\
&\quad + E_i^{[lfc,d]} \omega_i(k+l) \\
\hat{x}_i(k) &= x_i(k) \\
|\hat{x}_{i3}(k+l) - \hat{x}_{i2}(k+l)| &\leq T_{tb,i} \bar{p}_{mech} \\
\hat{u}_i(k+l) &\leq \bar{p}_{ref} \\
x_i(k) - \hat{x}_i(k) &\in \mathbb{Z}_i \\
\hat{x}_i(k+l) - \tilde{x}_i(k+l) &\in \mathbb{E}_i \\
\hat{x}_i(k+l) &\in \hat{\mathbb{X}}_i \\
\hat{x}_i(k+T) &\in \hat{\mathbb{X}}_i^F
\end{aligned} \tag{45}$$

for  $l = 0, \dots, T-1$ .

After each delegate obtains a solution to the optimization problem, the final assignment of  $u_{i, PoT}^*$  at the actuator side is similar to that in Supplementary Note 3 and is not repeated here. The power system in area- $j$  needs to transmit state information  $\hat{x}_j$  to area- $i$  via the blockchain network. Delegates of the blockchain network affiliated to each area will solve the above optimization problem in a given time and provide the final control command (load reference point) acted on the power system according to the PoT mechanism. Data interactions between areas are subject to internal dishonest behavior of the blockchain network and external cyber-attacks. Unlike traditional control methods, PoT-based LFC can greatly mitigate the interference of cyber-attacks on the frequency stability of power systems by means of active defense.

In order to quantify the trustworthiness of the data after it has been transmitted through the network, the security performance metric for the multi-area power system under load frequency control is set as follows

$$\begin{aligned}
H_{\alpha, lfc} &= \sum_{t=t_0}^{t_0+T} \left( \sum_{i=1}^N \left( \sum_{j \in \mathcal{N}_i^c} \left( \frac{1}{\Delta P_{tie,j,max}^{org}} |\tilde{x}_{ij}^P(t) - x_j^{P,org}(t)| + \frac{1}{\Delta f_{j,max}^{org}} |\tilde{x}_{ij}^f(t) - x_j^{f,org}(t)| \right) \right) \right. \\
&\quad \left. + \frac{1}{u_{i,max}^{org}} |\tilde{u}_i(t) - u_i^{org}(t)| \right)
\end{aligned} \tag{46}$$

where the meanings of the involved variables are presented in Supplementary Table 11. Variables  $\Delta P_{tie,j,max}^{org}$ ,  $\Delta f_{j,max}^{org}$  and  $u_{i,max}^{org}$  are used for normalization. Similarly, in order to quantify the performance of different load frequency control methods, the control performance metric of the system is designed as follows

$$J_{task,lfc} = \sum_{t=t_0}^{t_0+T} \sum_{i=1}^N \left( \frac{1}{ACE_{i,max}^{org}} |ACE_i^{org}(t)| + \frac{1}{u_{i,max}^{org}} |u_i^{org}(t)| \right) \tag{47}$$

where the meanings of  $t_0$ ,  $T$  and  $N$  are the same as those given in Supplementary Table 11, and the meanings of the remaining variables are explained in Supplementary Table 12.

Supplementary Table 11: Meanings of the variables in equation (46)

<b>Variable</b>	<b>Meaning</b>
$t_0$	Moment activating the specific load frequency control
$T$	Action time of the load frequency control strategy
$N$	Number of subsystems contained in the three-area power system
$x_j^{P,org}(t)$	Ideal power deviation value (i.e., ideal $\Delta P_{tie,j}(t)$ ) of subsystem $j$ in the three-area power system
$x_j^{f,org}(t)$	Ideal frequency deviation value (i.e., ideal $\Delta f_j(t)$ ) of subsystem $j$ in the three-area power system
$\tilde{x}_{ij}^P(t)$	Power deviation value actually used by the controller in the power system, which received by subsystem $i$ from subsystem $j$
$\tilde{x}_{ij}^f(t)$	Frequency deviation value actually used by the controller in the power system, which received by subsystem $i$ from subsystem $j$
$\tilde{u}_i(t)$	Control command actually used by the controller of subsystem $i$ in the power system
$u_i^{org}(t)$	Ideal control command of subsystem $i$ in the power system
$\Delta P_{tie,j,max}^{org}$	Maximum ideal power deviation value of subsystem $j$ during power system operation
$\Delta f_{j,max}^{org}$	Maximum ideal frequency deviation value of subsystem $j$ during power system operation
$u_{i,max}^{org}$	Maximum ideal control command of subsystem $i$ during power system operation

Supplementary Table 12: Meanings of the variables in equation (47)

<b>Variable</b>	<b>Meaning</b>
$ACE_{i,max}^{org}$	Maximum ideal area control error of subsystem $i$ during power system operation
$ACE_i^{org}(t)$	Ideal area control error of subsystem $i$ in the three-area power system, which is calculated from the measured power deviation and frequency deviation values



### VIII. SUPPLEMENTARY NOTE 5: DPOT-BASED CENTRALIZED SECONDARY REGULATION STRATEGY

The power system in this application is still a DC microgrid, so the system model involved is the same as that of Section V. Relying on the coupled large-signal model of the DC microgrid (20), the PFC-based secondary secure control with delay compensation is designed to be

$$\begin{aligned}
 u_{pfc,i}^c(t + \tau_{u,i}) &= g_i^I \sum_j a_{ij} ((h_{pre} \circ f_{pfc,y})(I_{so,j}(t)) - (h_{pre} \circ f_{pfc,y})(I_{so,i}(t))) \\
 &\quad + g_i^V \left( \frac{1}{N} \sum_{i=1}^N (h_{pre} \circ f_{pfc,y})(V_i(t)) - V^{ref} \right) \\
 u_{pfc,i}(t) &= f_{pfc,u}(u_{pfc,i}^c(t + \tau_{u,i}))
 \end{aligned} \tag{48}$$

where  $\tau_{u,i}$  is the time delay from controller to actuator,  $I_{so,i}(t) = I_{ti}(t)/\theta_i^s$ , it also applies to  $I_{so,j}(t)$ ,  $f_{pfc,y}$  and  $f_{pfc,u}$  denote the role of the PFC mechanism when transmitting measurements and control commands, respectively,  $g_i^I$  and  $g_i^V$  are the gains of current sharing and voltage recovery, respectively,  $h_{pre}$  the role of predictive control, and  $\circ$  the function composition. The rest of the unexplained variables have the same meaning as in Supplementary Note 3, e.g.,  $V_i(t)$ . It should be noted that the specific process for  $h_{pre}$  is available in previous work [16], [17], where the ideology is rolling predictions based on a system model.

Since the blockchain only provides secure transmission for the regulation of the DC microgrid and is not involved in the controller computation, the design of the secondary controller is not restricted by the PFC mechanism. As can be seen, this variant is low-cost to implement and can be readily embedded into existing controllers. There are various secondary secure control strategies based on PFC, and the controller (48) is just one of the examples given.

Similar to Application 1 and Application 2, the security performance metric of the DC microgrid in the centralised secondary control paradigm is given as

$$\begin{aligned}
 H_{\alpha,pfc} &= \sum_{t=t_{sec}}^{t_{sec}+T} \left( \sum_{i=1}^N \left( \left( \frac{1}{V_{i,max}^{org}} |\tilde{y}_i^V(t) - y_i^{V,org}(t)| + \frac{1}{I_{ti,max}^{org}} |\tilde{y}_i^I(t) - y_i^{I,org}(t)| \right) \right. \right. \\
 &\quad \left. \left. + \frac{1}{u_{i,max}^{org}} |\tilde{u}_i(t) - u_i^{org}(t)| \right) \right)
 \end{aligned} \tag{49}$$

where  $\tilde{y}_i^I(t)$  and  $\tilde{y}_i^V(t)$  represent voltage and current values of DGU  $i$  actually used by the centralized controller, respectively, the meanings of the other variables are the same as those in Supplementary Table 9. In order to evaluate the performance of various secondary control methods for accomplishing the regulation tasks given by (12) and (13), the control performance metric is defined as

$$J_{task,pfc} = \sum_{t=t_{sec}}^{t_{sec}+T} \left( \sum_{i=1}^N \left( \frac{1}{V_{i,max}^{org}} \left| \frac{1}{N} \sum_{i=1}^N V_i(t) - V^{ref} \right| + \sum_{j \in \mathcal{N}_i^c} \left( \frac{1}{I_{tj,max}^{org}} \left| \frac{I_{tj}^{org}(t)}{\theta_j^s} - \frac{I_{ti}^{org}(t)}{\theta_i^s} \right| \right) \right) \right) \tag{50}$$

where the meanings of the variables are shown in Supplementary Table 9 and Supplementary Table 10.

## SUPPLEMENTARY REFERENCES

- [1] A. Esmat, M. de Vos, Y. Ghiassi-Farrokhfal, P. Palensky, and D. Epema, "A novel decentralized platform for peer-to-peer energy trading market with blockchain technology," *Applied Energy*, vol. 282, p. 116123, 2021.
- [2] B. Lashkari and P. Musilek, "A comprehensive review of blockchain consensus mechanisms," *IEEE Access*, vol. 9, pp. 43 620–43 652, 2021.
- [3] W. Tushar *et al.*, "Peer-to-peer energy systems for connected communities: A review of recent advances and emerging challenges," *Applied energy*, vol. 282, p. 116131, 2021.
- [4] M. S. Sadabadi, N. Mijatovic, and T. Dragičević, "A robust cooperative distributed secondary control strategy for dc microgrids with fewer communication requirements," *IEEE Transactions on Power Electronics*, vol. 38, no. 1, pp. 271–282, Jan. 2023.
- [5] S. Trip, M. Cucuzzella, X. Cheng, and J. Scherpen, "Distributed averaging control for voltage regulation and current sharing in dc microgrids," *IEEE Control Systems Letters*, vol. 3, no. 1, pp. 174–179, Jan. 2019.
- [6] G. Duan, "High-order fully actuated system approaches: Part i. models and basic procedure," *International Journal of Systems Science*, vol. 52, no. 2, pp. 422–435, 2021.
- [7] Y. Yu, G.-P. Liu, and W. Hu, "Coordinated distributed predictive control for voltage regulation of dc microgrids with communication delays and data loss," *IEEE Transactions on Smart Grid*, vol. 14, no. 3, pp. 1708–1722, May. 2022.
- [8] M. Farina and R. Scattolini, "Distributed non-cooperative mpc with neighbor-to-neighbor communication," *IFAC Proceedings Volumes*, vol. 44, no. 1, pp. 404–409, 2011, 18th IFAC World Congress.
- [9] E. B. Curtis, D. Ingerman, and J. A. Morrow, "Circular planar graphs and resistor networks," *Linear Algebra and Its Applications*, vol. 283, no. 1-3, pp. 115–150, 1998.
- [10] R. Han, M. Tucci, A. Martinelli, J. M. Guerrero, and G. Ferrari-Trecate, "Stability analysis of primary plug-and-play and secondary leader-based controllers for dc microgrid clusters," *IEEE Transactions on Power Systems*, vol. 34, no. 3, pp. 1780–1800, May. 2019.
- [11] V. Nasirian, A. P. Yadav, F. L. Lewis, and A. Davoudi, "Distributed assistive control of power buffers in dc microgrids," *IEEE Transactions on Energy Conversion*, vol. 32, no. 4, pp. 1396–1406, Dec. 2017.
- [12] W. W. A. G. Silva, T. R. Oliveira, and P. F. Donoso-Garcia, "An improved voltage-shifting strategy to attain concomitant accurate power sharing and voltage restoration in droop-controlled dc microgrids," *IEEE Transactions on Power Electronics*, vol. 36, no. 2, pp. 2396–2406, Feb. 2021.
- [13] H. Bevrani, *Robust power system frequency control*, vol. 4. Springer, 2014.
- [14] T. H. Mohamed, J. Morel, H. Bevrani, and T. Hiyama, "Model predictive based load frequency control design concerning wind turbines," *International Journal of Electrical Power & Energy Systems*, vol. 43, no. 1, pp. 859–867, 2012.
- [15] M. Ma, H. Chen, X. Liu, and F. Allgöwer, "Distributed model predictive load frequency control of multi-area interconnected power system," *International Journal of Electrical Power & Energy Systems*, vol. 62, pp. 289–298, 2014.
- [16] G.-P. Liu, "Coordinated control of networked multiagent systems via distributed cloud computing using multistep state predictors," *IEEE Transactions on Cybernetics*, vol. 52, no. 2, pp. 810–820, 2022.
- [17] Y. Huang, G.-P. Liu, Y. Yu, and W. Hu, "Data-driven distributed predictive tracking control for heterogeneous nonlinear multiagent systems with communication delays," *IEEE Transactions on Automatic Control*, vol. 69, no. 7, pp. 4786–4792, 2024.